Geologica Acta, Vol.4, Nº1-2, 2006, 7-33
Available online at www.geologica-acta.com

geologica acta

Role of crustal melting in petrogenesis of the Cretaceous Water Island Formation (Virgin Islands, northeast Antilles Island arc)

W.T. JOLLY [1] and E.G. LIDIAK [2]

[1] Department of Earth Sciences, Brock University
St. Catharines, Ontario, Canada L2S 3A1. E-mail: wayne@brocku.ca

[2] Department of Geology and Planetary Science, University of Pittsburgh
Pittsburgh, PA, USA 15260 E-mail: egl+@pitt.edu

ABSTRACT

The latest Aptian to earliest Albian (~115 Ma) Water Island Fm in the Virgin Islands contains some of the oldest known arc-related strata in the Greater Antilles Island Arc. Hence, the unit is of considerable significance in tectonic reconstructions of initial subduction parameters along the long-lived destructive plate margin separating the North American and Caribbean Plates. Exposed Water Island strata are bimodal, consisting predominantly of altered dacite and rhyolite (originally called keratophyre; 65-85% SiO_2) and subordinate degraded (spilite; 46-57% SiO_2). TiO_2 content of Water Island basalt averages approximately 0.5%, resembling borderline intermediate-Ti boninite basalts, consistent with low incompatible element abundances and low normalized light rare earth elements (LREE) with respect to Sm. Trace element patterns of the felsic suite, characterized by pronounced negative normalized anomalies for high field-strength elements (HFSE), low Sr/Y, and low absolute rare earth element (REE) abundances, and relatively flat normalized REE patterns, have analogues in plagiorhyolite suites from bimodal Cenozoic arcs, including the western Aleutians, Izu-Bonin, the Kermadecs, and South Sandwich. Relatively low incompatible element concentrations in plagiorhyolites and contrasting normalized incompatible trace element patterns in basalts preclude an origin of Water Island plagiorhyolite through MORB-type fractional crystallization. Compositions are consistent instead with melting models involving partial fusion of amphibole-bearing gabbro at low pressures (within the stability range of plagioclase) in response to introduction of heat and aqueous flux by arc-related basalt melts and associated hydrothermal fluids during transmission to the surface. Truncation of the basalt fractional crystallization trend at SiO_2 = 57% indicates evolved island arc basalt (IAB) crystal fractionates were gradually displaced from crustal magma conduits by more buoyant plagiorhyolite melt, and trapped in underplated, sub-crustal magma chambers. Basalts have low $(Ce/Ce^*)_N$ (average ≈ 0.78), indicating the presence of significant pelagic sediment (0.5 to 1.5% Atlantic Cretaceous pelagic sediment, AKPS). One subunit of relatively high-HFSE plagiorhyolite has $(Ce/Ce^*)_N$ near-expected values, but another with low-HFSE has slightly lower than expected $(Ce/Ce^*)_N$, consistent with a small sediment component. Absence of intermediate andesite from the Water Island Fm is inconsistent, however, with basalt-rhyolite magma mixing processes. Consequently, incorporation of sediment by low-HFSE plagiorhyolite is inferred to have resulted from re-melting of arc-related gabbro.

KEYWORDS | Antilles. Virgin Islands. Water Island Fm. Plagiorhyolite. Crustal melting.

INTRODUCTION

The bimodal Water Island Fm, representing Late Aptian or Early Albian volcanic strata from the Antilles island arc in the Virgin Islands, is distinguished by the predominance of dacites and rhyolites (SiO_2 = 65 to 85 wt. %) over basaltic classes (SiO_2 = 45 to 55 %), and by the absence of intermediate andesites. The felsic rocks resemble leucocratic end-members of Cenozoic bimodal oceanic magma suites, named plagiogranites by Coleman and Peterman (1975), compositions of which are dominated by elevated SiO_2 and low Al_2O_3, Na_2O, MgO, Sr/Y<10, relatively flat chondrite normalized REE spectra, and negative normalized HFSE anomalies, reflecting a hydrous low pressure origin within the stability range of plagioclase (see for example Koepke et al., 2004). Plagiogranites are most common as small volume concentrations within veins, fractures and shear zones intruding oceanic crust sequences, such as the Southwest Indian Ocean Ridge (Hébert et al., 1991; Dick et al., 2000) and the Mid-Atlantic Ridge (Casey, 1997), as well as in ophiolite sequences of various ages (Gerlach et al., 1981; Jenner et al., 1991; Floyd et al., 1998; Koepke et al., 2004). The plagiogranite series was subsequently extended to include relatively larger concentrations of arc-related extrusive plagiorhyolite (Yazeva, 1978), also with low-Al_2O_3 and Sr/Y<10, similar to lavas reported from numerous Cenozoic arc terrains (Alabaster et al., 1982; Tsvetkov, 1991; Jafri et al., 1995; Tamura and Tatsumi, 2002; Leat and Lester, 2003; Leat and Smellie, 2003; Smith et al., 2003; Price et al., 2005). In addition, certain arc-related plagiogranite veins have adakitic compositions, characterized by elevated LREE, Al_2O_3, Sr/Y, low and strongly fractionated normalized HREE patterns with pronounced negative HFSE anomalies (Kamchatka Peninsula, Kepezhinskas et al., 1995; Drummond et al., 1996), reflecting an origin involving melting of garnet-clinopyroxene-bearing amphibolitized basalt at high water pressures within the descending slab (Rapp et al., 1999).

Pearce et al. (1984) found diversity within plagiogranites to be so great and representatives of group so widespread that trace element compositions of the rocks can be utilized to discriminate between various tectonic settings. Since similar compositional variations are observed in extrusive plagiorhyolite counterparts (Floyd et al., 1998; Koepke et al., 2004), a geochemical approach is also adopted here. Principal objectives include 1) examination of key major and trace element parameters on the basis of 32 new analyses of representative Water Island samples (Table 1, see Appendix), and 2) comparison of geochemical data with Cenozoic bimodal basalt-plagiorhyolite-bearing suites and experimental data, and 3) examination of the origin and tectonic setting of Water Island bimodality based on major and trace element fractional crystallization and partial melting models.

Basalt and plagiorhyolite end-members of the Water Island Fm, widely called spilites and keratophyres, respectively, to reflect their degraded, albite-chlorite-bearing secondary mineralogy (Donnelly and Rogers, 1980; Donnelly, 1989; Donnelly et al., 1990; Lebron and Perfit, 1994), are uniformly altered to assemblages consisting primarily of relict augite, albitized plagioclase, and chlorite. Experience has shown that most large-ion lithophile elements (LILE, including Rb, Ba, K, and Sr) are remobilized during low-temperature alteration, and that only Sr retains well-defined fields. To avoid confusion due to secondary compositional changes, geochemical models are restricted to the least soluble components, including rare earth elements (REE), high field-strength elements (HFSE), and Th (Pearce, 1983). The only exception is that Sr/Y is employed as a general indicator of melting pressures for entire rock populations.

GEOLOGICAL SETTING

The Antilles island arc platform is subdivided into two segments: 1) the Greater Antilles in the north and northwest, including Cuba, Hispañiola, Puerto Rico, and the Virgin Islands, all of which have been volcanically inactive since Paleogene time, and 2) the active Lesser Antilles in the east (Fig. 1). The northeast Antilles, including the Virgin Islands and Puerto Rico, occupies the region between these two arc sectors. Rocks representing the Jurassic pre-arc basement in the northeast Antilles are exposed both in central Hispañiola, where the Duarte Complex is comprised of obducted basaltic oceanic terrains (Draper et al., 1996; Lewis and Jiménez, 1991; Lapierre et al., 1997, 1999; Lewis et al., 1999, 2002), and in southwestern Puerto Rico (Fig. 1), where the Sierra Bermeja Basement Complex consists of serpentinized upper mantle ultramafic rocks, Lower Jurassic (~185 Ma) MORB tholeiite basalt (Lower Cajul Fm) and associated amphibolites (Las Palmas Amphibolite), and Jurassic to mid-Cretaceous chert (Mariquita Chert, Montgomery et al., 1994; Schellekens, 1998).

Limited paleontologic data from radiolarian chert (Donnelly, 1966), including new observations reported by Rankin (2002), indicate the Water Island Fm dates from Late Aptian or Early Albian time (~115 Ma, Rankin, 2002), which is in broad agreement with ages established in other islands (see summaries of Jolly et al., 1998a; Schellekens, 1998; Lewis et al., 2002). Island arc volcanism in the northeast Antilles continued episodically until mid-Eocene time (45 Ma, Frost and Schellekens, 1998).

Because oldest arc strata are of uniform age and because geochemical and lithological sequences are similar in all islands, the Antilles arc platform is considered to be remnants of a once continuous volcanic chain, possibly with multiple subduction zones, that formed along the western flank of the Pacific Plate and overrode the proto-Atlantic portion of the North American Plate as it swept eastward into the modern Caribbean (Burke, 1988; Donnelly, 1989; Pindell and Barrett, 1990; Draper et al., 1996; Lewis et al., 2002). Jolly et al. (this volume) suggested on geochemical grounds that subduction in the Virgin Islands involved young, and therefore pelagic sediment-poor, ridge-related oceanic crust generated along the southwest-trending Caribbean spur of the Mid-Atlantic Ridge (dated between 155 and 125 Ma, Pindell and Barrett, 1990) shortly following its extinction.

Stratigraphy in the Virgin Islands

The oldest strata in the Virgin Islands (Donnelly, 1966; Donnelly et al., 1971, 1990; Hekinian, 1971; Donnelly and Rogers, 1980), the bimodal Lameshure Volcanic-Intrusive Complex of Rankin (2002; Figs. 1 and 2), consist of between 2 and 4 km of extrusive volcanic rocks (Water Island Fm) and associated hypabyssal intrusive equivalents (Careen Hill Intrusive Suite). Water Island strata, which dips consistently northward, is widely exposed in south-eastern St. Thomas, eastern St. John, and on Norman and Peter Islands in the east (Fig. 2). Predominant felsic end-members, comprising approximately 80% of the unit (Rankin, 2002), range from dacites to siliceous rhyolites (65 to 88% SiO_2 on a volatile-free basis), whereas subordinate mafic end-members (20%) are largely restricted to the basaltic range (46 to 57% SiO_2). The various units of the formation are commonly interlayered, but thick uninterrupted sequences of both types are present (Fig. 2). Basaltic strata are dominated by aphanitic to sparcely porphyritic, amygdaloidal and commonly pillowed, plagioclase-ferroaugite-bearing lava, lava breccia and tuff, together with related intrusive feeder dikes and stocks and pelagic radiolarian chert. Analyzed basaltic rocks include representative non-amygdular lavas and individual clasts separated

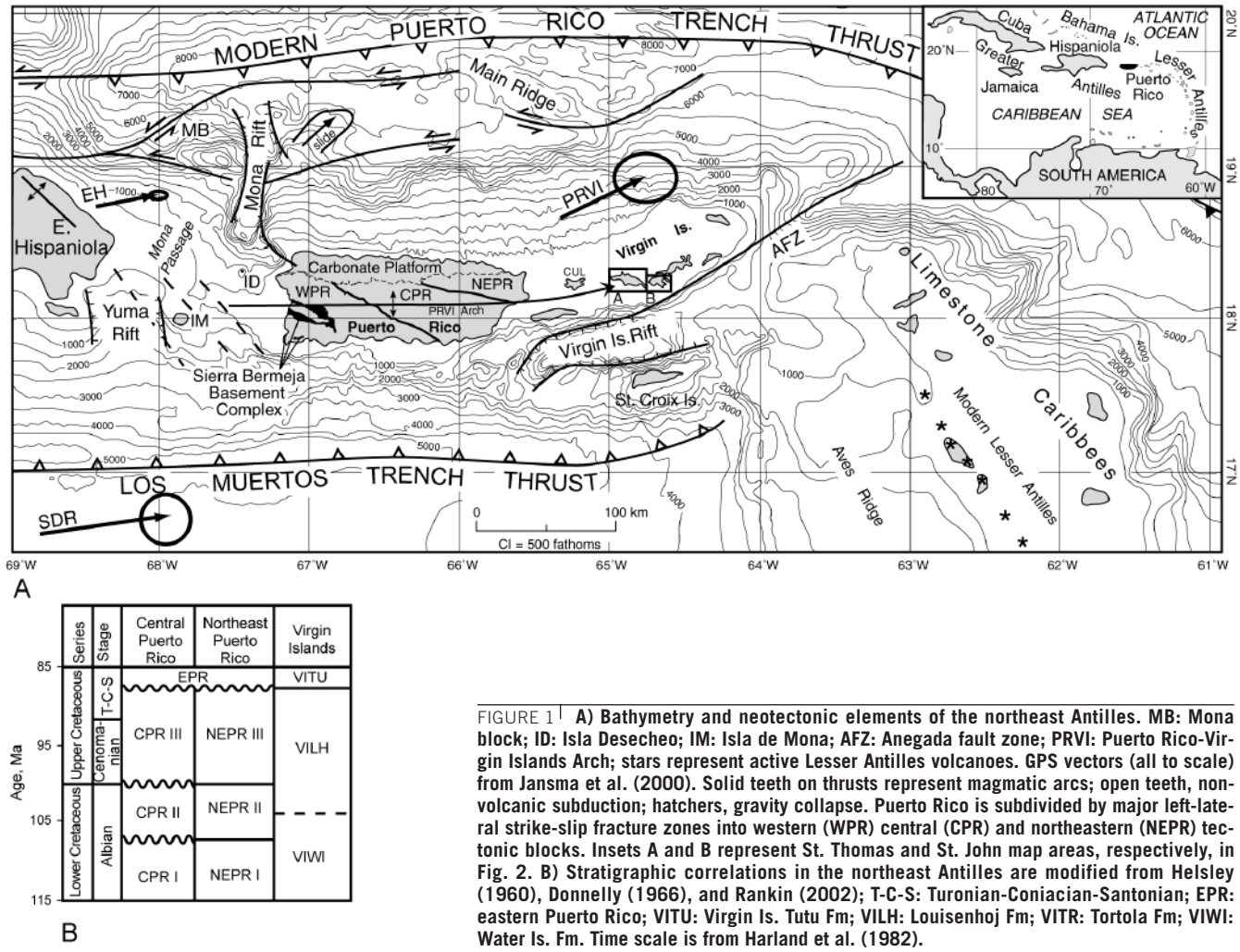

FIGURE 1 | **A) Bathymetry and neotectonic elements of the northeast Antilles. MB: Mona block; ID: Isla Desecheo; IM: Isla de Mona; AFZ: Anegada fault zone; PRVI: Puerto Rico-Virgin Islands Arch; stars represent active Lesser Antilles volcanoes. GPS vectors (all to scale) from Jansma et al. (2000). Solid teeth on thrusts represent magmatic arcs; open teeth, non-volcanic subduction; hatchers, gravity collapse. Puerto Rico is subdivided by major left-lateral strike-slip fracture zones into western (WPR) central (CPR) and northeastern (NEPR) tectonic blocks. Insets A and B represent St. Thomas and St. John map areas, respectively, in Fig. 2. B) Stratigraphic correlations in the northeast Antilles are modified from Helsley (1960), Donnelly (1966), and Rankin (2002); T-C-S: Turonian-Coniacian-Santonian; EPR: eastern Puerto Rico; VITU: Virgin Is. Tutu Fm; VILH: Louisenhoj Fm; VITR: Tortola Fm; VIWI: Water Is. Fm. Time scale is from Harland et al. (1982).**

from tuff breccias. Felsic end-members are fine-grained spherulitic lavas that are commonly layered, brecciated, and extensively hydrothermally altered. The Water Island Fm is intruded by numerous younger, predominantly fine-grained to porphyritic basaltic dikes, sills, and stocks, many of which are identified by the presence of epidote-bearing metamorphic aureoles (Rankin, 2002).

At several localities the Water Island Fm grades conformably upward (Rankin, 2002) to lava, volcanic breccia and conglomerate, sand, and tuffaceous shale of the succeeding Louisenhoj Fm (Donnelly, 1966). This unit, between 0.5 and 1.5 km thick, consists primarily of fragmental extrusive basalt accompanied by appreciable proportions of both andesite and rhyolite. Louisenhoj volcanism was followed conformably by deposition of the Outer Brass Limestone, a platform carbonate dated by planktonic Foraminifera to between Late Turonian and Late Santonian time (~85 Ma, Pessagno, 1976). Succeeding, also conformable, volcanic sandstone, shale, and conglomerate of the Tutu Fm, of Santonian to Campanian age (Donnelly, 1966), are restricted to a narrow belt on the north side of the islands (Fig. 2). Strata in northern St. John were metamorphosed to hornblende-garnet amphibolite by the calcalkaline Virgin Islands Batholith and satellite plutons (Fig. 2; Helsley, 1960; Donnelly and Rogers, 1980; Donnelly et al., 1990; Lidiak and Jolly, 1996). The intrusive rocks, representing the final major magmatic event in the northeast Antilles, have Oligocene K/Ar (Cox et al., 1977) and $^{40}Ar/^{39}Ar$ (Rankin, 2002) radiometric ages ranging from 35 to 39 Ma.

Petrography of Water Island lavas

Basalts from the Water Island Fm are essentially aphyric to slightly porphyritic, with small (1 to 5 mm long) and sparce augite and mostly albitized plagioclase phenocrysts in an aphanic groundmass of devitrified and chloritized glass, feathery-textured clinopyroxene, and

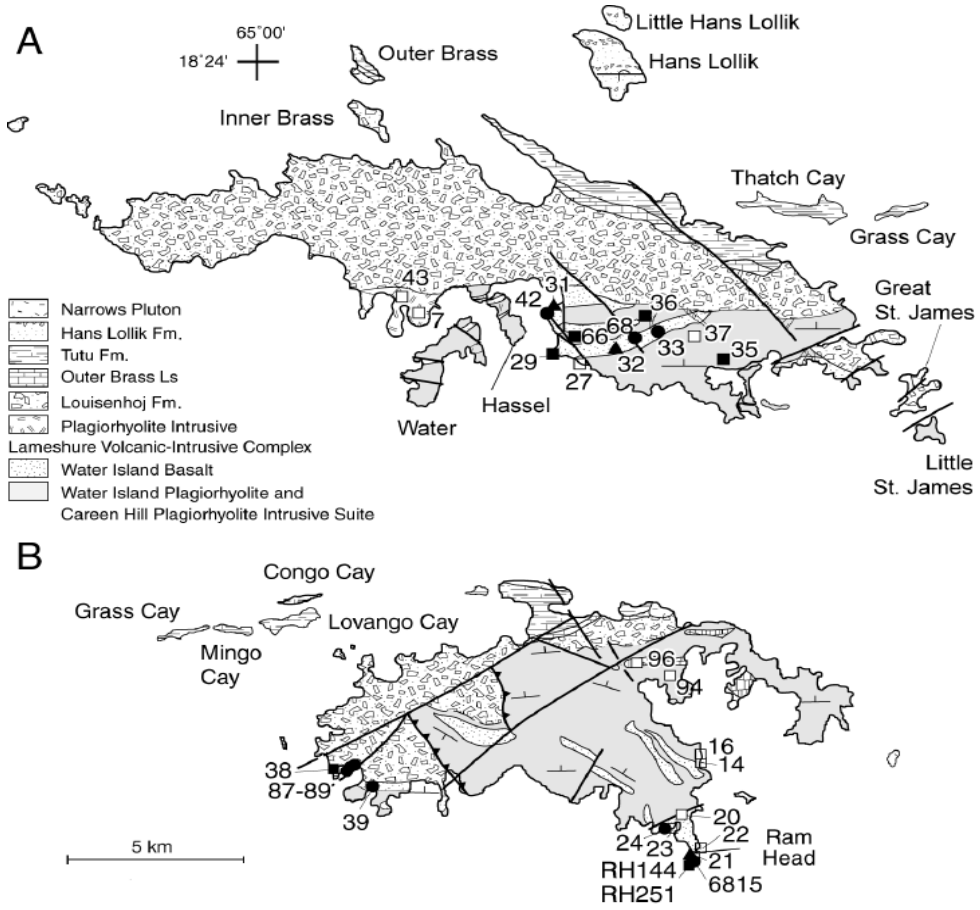

FIGURE 2 | **Geologic maps of St. Thomas (A) and St. John (B), US Virgin Islands, showing location and subunit designations of analyzed Water Island samples; geology from Donnelly (1966) and Rankin (2002). Subunits identified in Fig. 3 as follows: solid circle, low-HFSE borderline boninitic basalt (VIWI-1); solid square, low-HFSE plagiorhyolite (VIWI-4); square, high-HFSE plagiorhyolite (VIWI-5); solid pyramid MORB-like basalt (VIWI-3). Strike and dip symbols indicate attitude of bedding, heavy lines represent faults, teeth on faults indicate overthrusting. Note the maps are at the same scale and overlap at Grass Cay.**

quenched albitized feldspar microlites. Accessory titanomagnetite is ubiquitous, pseudomorphs of olivine are present in a few samples, and green spinel is a trace component in altered rocks. Most of the rocks were strongly hydrated (chloritized) during alteration. In addition abundant prehnite and rare pumpellyite are present as low-temperature alteration products (see also Rankin, 2002).

Like basaltic end-members, Water Island plagiorhyolite are predominantly aphanitic. However, albitized plagioclase laths and euhedral to subhedral quartz, both of which range in length from 0.5 to 5 mm, as well as tiny magnetite grains, appear in many of the samples studied. Rankin (2002) subdivided eruptive plagiorhyolites into three textural types: (1) phenocryst-poor aphanitic rocks with less than 10% plagioclase plus quartz crystals (including samples 14, 20, 21, 22, 27, 35, 37, and 66 in Table 1), which comprise almost 90% of the plagiorhyolite suite; (2) plagioclase-quartz porphyries with between 10 and 25% plagioclase plus quartz phenocrysts (samples 7, 16, 25, 29, and 36, 43), comprising up to 10% of the suite; and (3) rare plagioclase-phyric varieties with between 5 and 10% plagioclase crystals (samples 38 and 23). Mineralogy of analysed plagiorhyolite samples is compared to bulk rock compositions in Fig. 3B (see symbols denoted a, b, etc.).

GEOCHEMISTRY OF THE BIMODAL WATER ISLAND FORMATION

Data base, analytical methods, and geochemical parameters

Major (ICP-ES) and trace element (ICP-MS) analyses from 32 Water Island samples (15 basalts and 17 plagiorhyolites) are provided in Table 1; sample locations are included in Fig. 2. Supplementing Water Island data (Table 2, see Appendix) are 12 analyses of pre-arc MORB tholeiite basalt and trondhjemite fractionates, and a representative of the associated Las Palmas Amphibolite, both from Arroyo Cajul in the Sierra Bermeja Complex, western Puerto Rico (Schellekens et al., 1990; Jolly et al., 1998a and b). Rock analysis was performed by Acme Analytical Laboratories at Vancouver, BC, Canada. Sample preparation and analytical methods are outlined in Jolly et al. (this volume). To avoid scatter introduced by secondary hydration, data in diagrams and theoretical models (but not in Tables 1 and 2) are recalculated on a volatile-free basis.

Spinel peridotite melting models were calculated as described in Jolly et al. (this volume). In conformity with Nb and Yb abundances (figs. 10 and 11 of Jolly et al., this volume) and Cr/Yb relations, models were calculated for 25% fusion (f = 0.25). Starting compositions were selected from the range of mantle compositions suggested by Pearce and Parkinson (1993) and modified by Bédard (1999), whereas compositions of Atlantic Cretaceous pelagic sediment (AKPS) are from Jolly et al. (this volume). Chondrite values and the order of incompatible elements are from Sun and McDonough (1989).

Partition coefficients for mantle melting processes in spinel peridotite are modified from Pearce and Parkinson (1993) and Bédard (1999), while those for equilibrium batch melting and basaltic fractional crystallization are from Rollinson (1993). Published coefficents (D-values) for HFSE partitioning between felsic liquids and residual ilmenite (ilm) have an exceedingly large range. For example, $D^{ilm}/_{Nb}$ reported by Ewart and Griffin (1994) and Stimac and Hickmott (1994) range from 6.58 to 89.9 and from 50.9 to 64.2, respectively. In comparison, a similar range, $D^{ilm}/_{Ta}$ = 64 to 85, was reported by Stimac and Hickmott, while a higher average of 106 was suggested for that element by Nash and Crecroft (1985). Stimac and Hickmott also reported a large range of $D^{ilm}/_{Ti}$, from 150 to 235, but Sisson (1991) indicated lower values, averaging 16.5. An experimental value of $D^{rutile}/_{Ta}$ = 44 was measured in intermediate liquids by Green and Pearson (1987). Values of 50 and 100 for Nb and Ti, respectively, representing the mid-range of published values, are adopted here for use in melting and fractional crystallization models.

Geochemical terminology

Previous geochemical classifications of island arc basalts in the Virgin Islands, and elsewhere in the Greater Antilles, subdivided the rocks into two groups (Fig. 3) based on isotope data, normalized REE slopes, and relative abundances U, Th, and large-ion lithophile elements (LILE, K, Rb, Sr, Ba; Donnelly and Rogers, 1980; Donnelly, 1989; Donnelly et al., 1990; Lebron and Perfit, 1994): 1) a lower primitive island arc suite (PIA) with low incompatible elements and radiogenic isotope abundances, consisting predominantly of degraded, albite-bearing low-K basalt (spilite) accompanied, in the Water Island Fm, by altered quartz-albite-bearing dacite and rhyolite (originally called keratophyre) and 2) an overlying basalt to intermediate calc-alkaline suite (CA), with elevated incompatible and radiogenic element concentrations, consisting primarily of andesite and related crystal fractionates.

PIA-type lavas typically have low LILE, LREE, and HFSE abundances, low Th, U, and radiogenic Pb, and near-horizontal or slightly depleted normalized LREE spectra. Hence, trace element distribution is broadly equivalent to the conventional modern island arc tholeiite (IAT) series (Jakeš and Gill, 1970). Younger CA-type

lavas, distinguished from PIA by elevated LREE, U, Th, and radiogenic Pb abundances, resemble the orogenic calcalkaline series of Gill (1981). Jolly et al. (this volume) concluded REE content of Antilles volcanic rocks is closely related to proportions of subducted pelagic sediment, which is highly variable, both temporally and spatially, across the northeast Antilles. Moreover, recent geochemical investigations revealed many PIA basalts in the Greater Antilles, including the Téneme Fm in Eastern Cuba (Proenza et al., this volume), and the Maimon Fm in central Hispañiola (Horan, 1995; Lewis et al., 2000, 2002), as well as Water Island basalts, have boninitic affinities (low TiO_2, Al_2O_3, CaO, and REE, especially heavy rare earth elements (HREE), compared with IAB and MORB basalts), indicating anomalous, incompatible element-depleted mantle source compositions (Hickey and Frey, 1982; Crawford, 1989; Pearce and Parkinson, 1993; Bédard, 1999). On A TiO_2 vs. FeO*/MgO plot (Fig. 4B), total Fe calculated as FeO*), the Tenemé Fm plots within the intermediate-Ti boninite field of Bédard (1999), whereas Water Island basalts (VIWI-1, -2, and –3), with an average of approximately 0.5% TiO_2, plot along the boundary between intermediate-Ti boninites and IAB; hence, the rocks are considered to be boninitic rather than true boninites. In comparison, rocks stratigraphically correlated with the Water Island Fm from central Puerto Rico (Fms A, B, and C, Jolly et al., 2001, 2002, this volume) are restricted to the combined IAB-MORB field, with $TiO_2 > 0.5\%$.

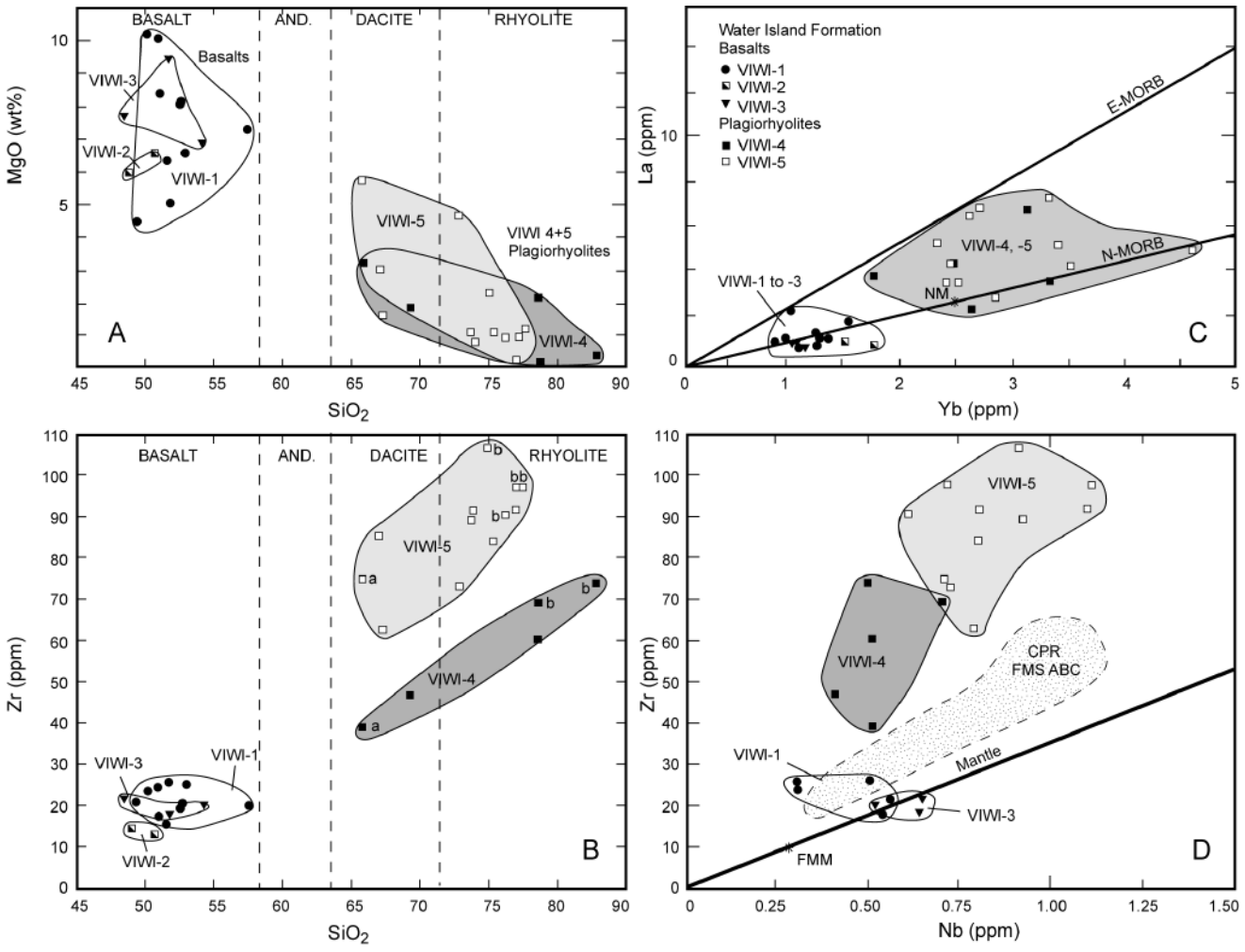

FIGURE 3 | **Geochemical subdivision of Water Island Fm from covariation of critical major and incompatible elements. A) SiO_2 -MgO illustrates the absence of intermediate andesite from the Water Island bimodal basalt-plagiorhyolite assemblages. Volcanic classes are based on SiO_2 content, according to the classification system of La Maitre (1989); basaltic andesite (SiO_2 = 52 to 57%) are included in the basalt range and the dacite-rhyolite boundary is set at 72% SiO_2. Both dacite and rhyolite are included within the plagiorhyolite – plagiorhyolite series (Coleman and Peterman, 1975; Coleman and Donato, 1979). B) SiO_2 - Zr discriminates low- and high-HFSE plagiorhyolites. C) Water Island basalts and plagiorhyolites lie between the N-MORB and E-MORB trends in Yb-La plots. D) MORB-like basalts and high-LREE basalts both lie along the N-MORB trend (Sun and McDonough, 1989) in Nb-Zr plots; in comparison, equivalent volcanic strata from Formations A, B, and C in central Puerto Rico have a higher slope and elevated Nb. FMM represents the fertile MORB-type source of Pearce and Parkinson (1993).**

Geochemical subdivision

Basalts, with Zr concentrations ranging from <10 to approximately 30 ppm, form a tight cluster between 48 and 57% silica on Zr-SiO_2 plots (Fig. 3B). The rocks are resolved into three subunits, one with low Nb (designated basalt subunit VIWI-1), another (VIWI-2) from the sheeted dike complex in southern St. John (Rankin, 2002) with Nb concentrations below the analytical detection limit (0.5 ppm), and a third (VIWI-3) with MORB-like chondrite-normalized incompatible element patterns. Together the basalts form a tight, moderately negative field on CaO/Al_2O_3 vs FeO*/MgO diagrams (Fig. 4A), reflecting high-pressure, cpx-dominated fractional crystallization. The trend contrasts with low negative slopes characteristic of low-pressure, plagioclase-dominated MORB fractional crystallization (Yogodzinski et al., 1995). As indicated above, Water Island boninitic basalts (VIWI-1, -2 and -3) have somewhat depleted Ti and Yb concentrations compared with N-MORB, ranging from 0.45 to 0.65 % TiO_2 (average approximately 0.5%) and 1.0 to 1.5 ppm Yb, respectively (Fig. 4B and 4C). A graphic core-log presented by Hekinian (1971), representing the exclusively basaltic upper 360 m of a 740 m log drill core recovered from the vicinity of Ram Head, St. John (Fig. 2B), indicates the rocks have similar intermediate-TiO_2 concentrations average ~0.5%.

Water Island plagiorhyolites, like the interlayered basalts, are characterized by low HFSE, especially Nb, Ta, and Ti. In addition, most samples have low MgO (<3%), total REE and LREE (La<8 ppm; Fig. 3C), Sr, and Sr/Y<10). Al_2O_3 content and CaO/Al_2O_3 Water Island plagiorhyolites are also low (averaging 12.8% and 0.2, respectively, Table 1 and Fig. 4A) compared with Antilles basalts of equivalent age (averaging = 17.6% and 0.75 in Fm A basalts from central Puerto Rico; Jolly et al., 2001, this volume). The rocks form discrete low-HFSE (VIWI4) and high-HFSE (VIWI5) groups on Zr-SiO_2 plots, with low-HFSE varieties ranging from 40 to 70 ppm Zr, compared to a range from 60 to 110 ppm in high-HFSE types.

Geographic distribution of geochemical subunits

Basalt is present throughout the Water Island Fm, commonly interlayered with plagiorhyolite, but more significant concentrations occur in three geographic areas of the northern Virgin Islands (Fig. 2). The most extensive exposures are in southeastern St. John (Fig. 2B), where, for example, the upper 360 m of the Ram Head drill core is composed entirely of basalt and gabbro (Hekinian, 1971). Isolated domains of basalt strata are also present within plagiorhyolite further north where the rocks are largely inaccessible within Virgin Islands National Park. Basalt predominates in two additional areas below the transitional contact with the Louisenhoj Fm, one in southwestern St. John and another in southeastern St. Thomas (Fig. 2A).

Distribution of the two Water Island plagiorhyolite subunits (VIWI-4 and -5) appears geographically controlled. Low-HFSE types are present exclusively in southeastern St. John in the vicinity of Ram Head (Fig. 2B), and in the two areas below the Louisenhoj Fm in western St. John and St. Thomas, in areas dominated by basalt. North of an east northeast-trending fault zone (Fig. 2B) that separates the Ram Head area from eastern St. John, basalts are relatively more scarce, and low-HFSE plagiorhyolite is absent, and is replaced by high-HFSE types. Correlations across the fault are uncertain (Rankin, 2002), and it is possible the entire stratigraphic section in northeast St. John is repeated on the south side.

Chondrite-normalized incompatible element patterns

Normalized incompatible element patterns of boninitic basalts (VIWI-1 and –2; Fig. 5C) have moderately La enriched normalized LREE slopes, low Yb_N (5 to10), low Zr and Nb abundances with negative Zr and Nb anomalies, and a pronounced negative Ce-anomaly, but the rocks have no significant Eu anomaly. The Water Island Formation contains a small proportion of MORB-like basalts (VIWI-3) that (1) plot along the N-MORB line on binary diagrams involving HFSE (Fig. 3D) and (2) have relatively smooth, flat normalized middle rare earth elements (MREE)-HREE segments. Incompatible element concentrations overlap boninitic basalts, except for smaller chondrite-normalized Nb-anomalies (Fig. 5).

All Water Island plagiorhyolites (VIWI-4 and -5) have relatively flat normalized incompatible element spectra (Fig. 5A and B) characterized by the presence of negative normalized Nb, Ta, and Ti anomalies. Low-HFSE plagiorhyolites, which have moderate Zr and extremely deep Nb- and Ti-anomalies, comprise two subgroups, one (VIWI4a, consisting of samples 66 and 35, Fig. 5A and Table 1) with moderate negative Ce-anomalies and slightly enriched normalized LREE slopes, and another (VIWI4b, samples 66, 29, and 37) with relatively flat LREE segments. In comparison, high-HFSE plagiorhyolites have relatively shallower Nb- and Ta-anomalies, lack Ce- and Zr-anomalies, but have deeper negative Ti-anomalies and lower TiO_2 than low-HFSE types (VIWI-4). Both plagiorhyolite subunits have high Yb_N, ranging from 10 to approximately 30.

GEOCHEMICAL AFFINITIES OF WATER ISLAND PLAGIORHYOLITES

Comparison with Cenozoic high-pressure slab melts (adakites)

In covariation plots of SiO_2 vs. molar Mg/[Mg+Fe], the low-SiO_2 part of the Water Island plagiorhyolite field (Fig. 6C) overlaps the adakite series (Kay, 1980), which is an integral part of volcanic suites in numerous Cenozoic arcs. Examples include the western Philippines (Sajona et al., 1994), Panama (Defant et al., 1991), the Aleutians (Kay, 1980; Yogodzinski et al., 1994, 1995), Chile (Stern and Kilian, 1996), and Japan (Morris, 1995; Tamura and Tatsumi, 2002; Tatsumi et al., 2003), but many others have been reported. Water Island plagiorhyolites also partly overlap the field of the Archean plutonic tonalite-trondhjemite-granodiorite series (TTG of Barker, 1979; Martin, 1986), as defined by Smithies (2000; Fig. 6B), which closely resemble low-Mg-type extrusive Cenozoic adakites.

Adakite compositions, characterized by intermediate SiO_2, and high Al_2O_3, Sr, Sr/Y<100, and fractionated normalized HREE slopes with low Yb (Defant and

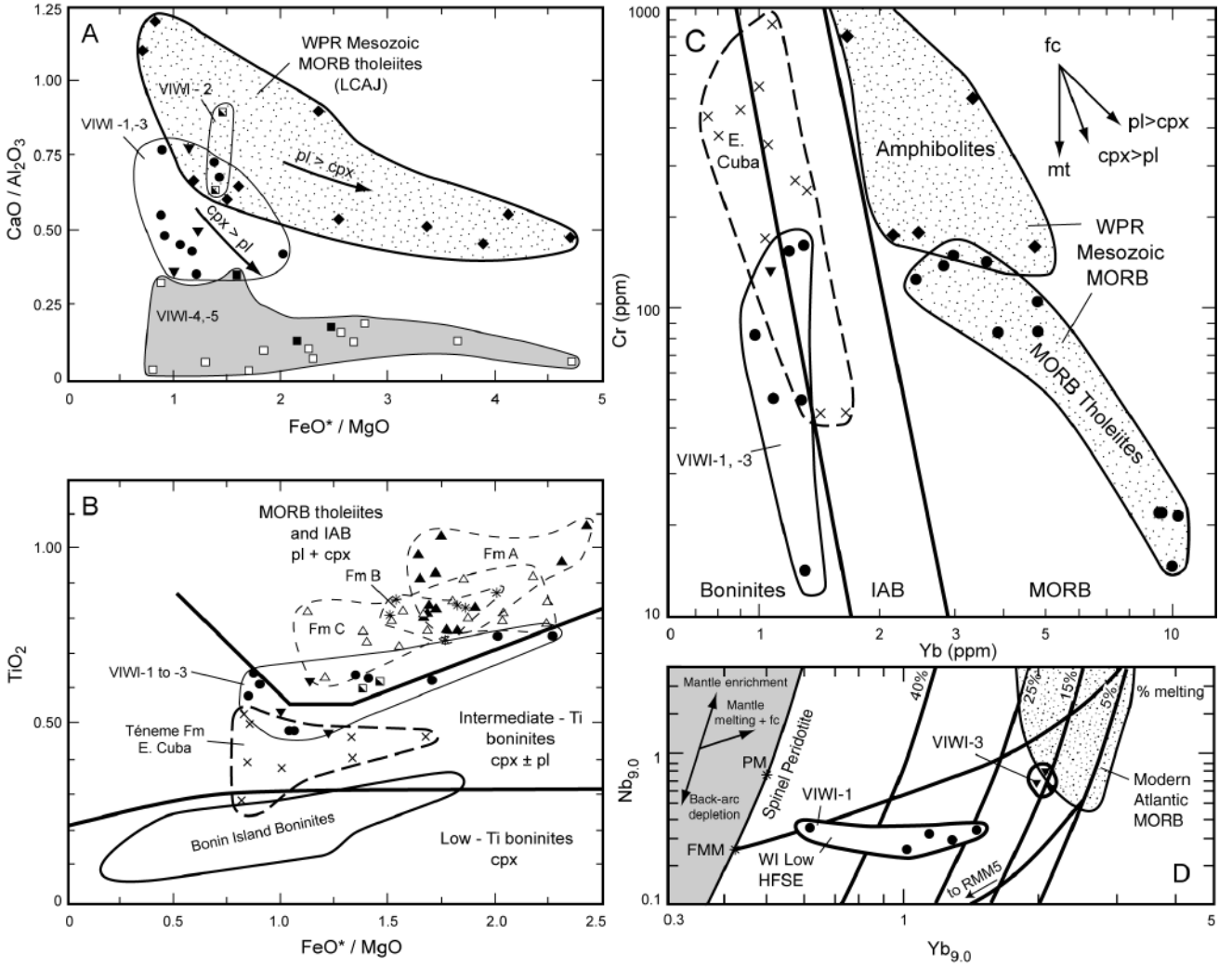

FIGURE 4 | **Petrogenetic processes in the Water Island Fm. A) CaO/Al_2O_3 vs. FeO*/MgO differentiates MORB from IAB type fractional crystallization series, and the field of plagiorhyolites. LCAJ identifies the tholeiitic field of the lower Cajul Fm, southwest Puerto Rico, which represents western Puerto Rican (WPR) pre-arc MORB. B) TiO_2 - Fe*/MgO discriminates low- and intermediate-Ti boninites according to the classification of Bédard (1999; temporal correlatives of the Water Island Fm in central Puerto Rico (Formations A, B, and C) are from Jolly et al. (2001, 2002; this volume); Bonin Island field is from Crawford (1989); Téneme Fm data are from Proenza et al. (this volume); Fe* represents total Fe as FeO; WPR Mesozoic MORB includes extrusive tholeiites from the Cajul Fm and amphibolites from the Las Palmas Amphibolite, southwest Puerto Rico. C) Yb vs Cr discriminates boninites, IAB, and MORB basalts (Pearce and Parkinson, 1993); units are identified as in B. Fractional crystallization (fc) vectors are included for opaque oxides (mt), for melts in which clinopyroxene (cpx) is greater and less than plagioclase (pl).) Yb9.0 and Nb9.0 represent corrected elemental abundances at MgO = 9.0 (see Jolly et al., this volume). D) Theoretical melting curves (from Pearce and Parkinson, 1993) for melting of fertile MORB mantle (FMM) and 5% depleted mantle (RMM5; Pearce and Parkinson, 1993) are indicated together with contours representing degree of melting. Modern MORB field is from data of Dosso et al. (1993).**

Drummond, 1990), indicate an origin through melting of amphibolite at elevated pressures above the stability range of feldspar, a process consistent with residual clinopyroxene and garnet in the source (1-4 GPa, Beard and Lofgren, 1991; Wyllie and Wolf, 1993; Sen and Dunn, 1994; Rapp and Watson, 1995; Rapp et al., 1999; Proteau et al., 2001). It is difficult to independently assess mineral-melt equilibria for Water Island volcanic rocks, since normative values are unreliable due to low-temperature alteration. In many significant respects, however, Water Island plagiorhyolites, characterized by low Sr/Y < 10, Sr, Al_2O_3 (Table 1), and relatively flat normalized HREE slopes (Figs. 5Aand 5B), represent the opposite end of the compositional spectrum relative to adakites (Fig. 7).

Cenozoic bimodal basalt-plagiorhyolite associations

The geochemistry of Water Island plagiorhyolites more closely resembles bimodal basalt-plagiogranite suites of various petrogenetic derivations, such as representatives from ophiolites, where the felsic rocks form small-volume veins that are predominantly but not exclusively leucocratic (Coleman and Donato, 1979; Hopson et al., 1981; Pallister and Knight, 1981; Alabaster et al., 1982; Pearce et al., 1984; Barbieri et al., 1994; Floyd et al., 1998), and in Cenozoic oceanic crust sequences (Carmichael, 1964; Coleman and Peterman, 1975; Flagler and Spray, 1991; Floyd et al., 1998; Jafri et al., 1995; Koepke et al., 2004). Larger concentrations of extrusive plagiorhyolite with similar compositions are reported from Cenozoic subduction-related island arcs, including the Aleutians (Tsevtkov, 1991), Izu-Bonin (Tamura and Tatsumi, 2002), Tonga-Kermadec (Smith et al., 2003), and South Sandwich (Leat et al., 2003). Plagiorhyolite is also reported from Mesozoic and Paleozoic arc settings, such as the Urals (Yazeva, 1978) and Bay of Islands, Newfoundland (Malpas, 1979; Elthon, 1991; Jenner et al., 1991; Bédard, 1999). In certain arc settings (cf., Canyon Mountain, Oregon, Gerlach et al., 1981) basalt is replaced by andesite as the mafic end-member. Although sometimes utilized to describe veins with adakite compositions (Kepezhinskas et al., 1995; Drummond et al., 1996), the term plagiorhyolite is restricted here to rocks with low Al_2O_3, Sr, Sr/Y<10, relatively low total REE and relatively flat normalized HREE patterns.

Many authors (Malpas, 1979; Gerlach et al., 1981; Floyd et al., 1998; Bédard, 1999; and Koepke, 2004) distinguished a pair of distinctive plagiorhyolite series. The two are difficult to distinguish on the basis of major element criteria alone (Koepke et al., 2004),

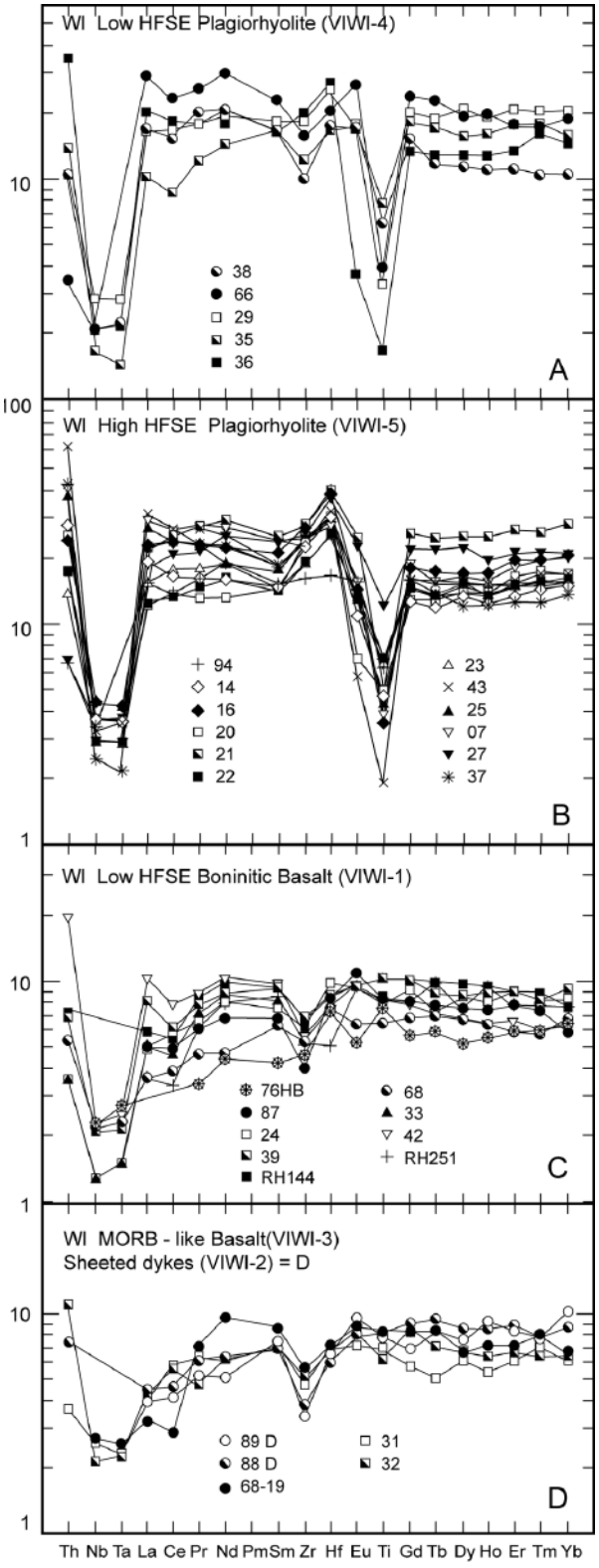

FIGURE 5 | **Chondrite-normalized incompatible element patterns from Water Island subunits. A) Low-HFSE plagiorhyolites (VIWI-4). B) High-HFSE plagiorhyolites (VIWI-5). C) Boninitic basalt (VIWI-1). D) Sheeted dikes (VIWI-2, denoted D) and MORB-like basalt (VIWI-3). Normalization values are from Sun and McDonough (1989); all patterns are presented at the same scale.**

but can be differentiated utilizing normalized REE spectra into 1) a high REE, fractional crystallization-related Samail-type series and 2) a relatively low REE, partial melting-related Canyon Mt-type series. Plagiorhyolite of the Samail-type, named for ophiolites in Oman (Coleman and Donato, 1979), is potentially represented in the Antilles by tholeiitic trondhjemite from the western Puerto Rican Mesozoic MORB suite (Fig. 8A), whereas the Canyon Mt-type is potentially represented by Water Island plagiorhyolites, which resemble Cenozoic arc-related plagiorhyolite suites with respect to both major (SiO_2 and molar Mg/[Mg+Fe], Fig. 6D) and incompatible trace element concentrations (Sr/Y-Y, Fig. 7).

Numerous experimental studies, mostly at 1 atm in the dry system, reveal that fractional crystallization of Fe-Ti-oxide rich assemblages produce Samail-type siliceous melts from a tholeiitic parent (Juster et al., 1989, Thy and Lofgren, 1994; Toplis and Carroll, 1995). In contrast, melts resembling Canyon Mountain-type plagiorhyolites were generated experimentally Baker and Eggler (1987), Housch and Luhr (1991), Beard (1995), and Koepke et al. (2004) in wet gabbro at crustal pressures. Koepke et al. (2004) produced such melts at 200 MPa and temperatures between 900 and 940º C, Fig. 6D. Low-Ti starting material used in the runs precluded production of Ti-Nb-oxide phases (Koepke et al., 2004), but other authors (Ryerson and Watson, 1987; Hirose, 1997) reported residual opaque phases in wet low pressure experiments (1 KPa), consistent with negative Ti- and Nb-anomalies in plagiorhyolite.

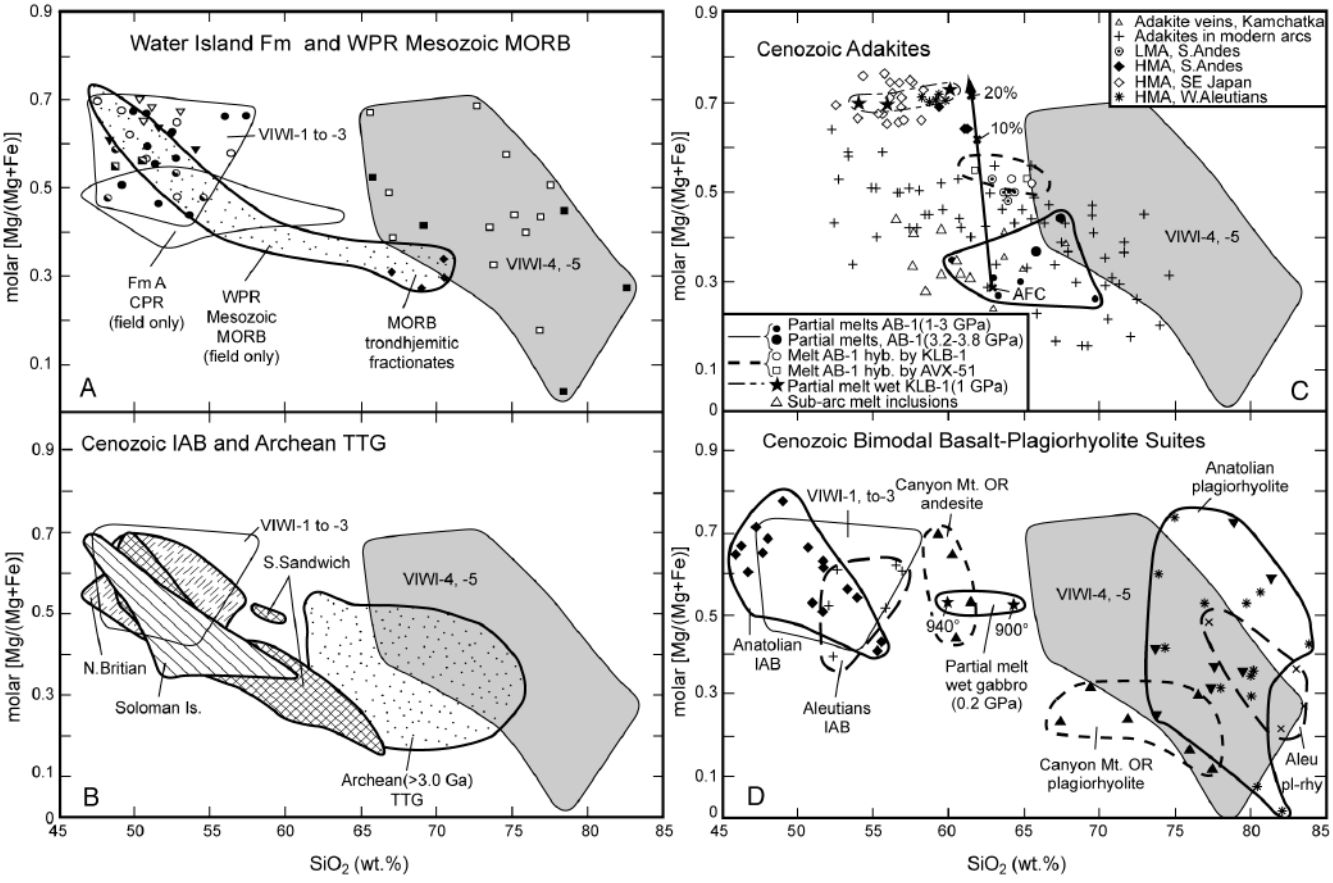

FIGURE 6 | **Covariation of SiO_2 and molar Mg/[Mg+Fe] = Mg#/100. A) Water Island Fm (symbols as in Fig. 3; plagiorhyolite field shaded) and field of western Puerto Rican MORB (stippled); four trondhjemitic crystal fractionates identified by diamonds. Also included for comparison is the field of equivalent central Puerto Rican IAB from Formation A (Jolly et al., 2002, this volume), which overlaps the lower part of the Water Island basalt field. B) Fields of selected Cenozoic mid-oceanic (low sediment) island arcs, including New Britian (Woodhead et al., 1998), Soloman Islands (Pearce et al., 1999), South Sandwich Is. (Pearce et al., 1995), and the Archean tonalite-trondhjemite-granodiorite (TTG) suite (>3 Ga, Smithies, 2000), compared with VIWI. C. Global adakites, experimental melts of amphibole basalt (1 to 4 GPa, Rapp et al., 1999) and hydrous peridotite (1 GPa, Hirose, 1997), and analyzed sub-arc melts from peridotite xenoliths (Schiano and Clocchiatti, 1994; Schiano et al., 1995), compared with Water Island plagiorhyolite (VIWI4 and 5). See text and Rapp et al. (1999) for data sources. Symbols as follows: AB: amphibole basalt; KLB-1: depleted peridotite; AVX-1: incompatible element enriched peridotite; LMA: low-Mg adakite; HMA: high-Mg andesite; AFC: simultaneous mantle assimilation and fractional crystallization (Stern and Killian, 1996). D. Cenozoic basalt-plagiorhyolite suites compared to the Water Island plagiorhyolite, see text for sources. Experimental melts of wet gabbro are indicated for 900 and 940°C at PH_2O = 200 MPa (Koepke et al., 2004).**

PETROGENESIS OF THE WATER ISLAND BASALT-PLAGIORHYOLITE SUITE MORB-THOLEIITE FRACTIONAL CRYSTALLIZATION RESIDUAL (SAMAIL-TYPE) MODELS

Major element mass balance calculations

Koepke et al. (2004), who compiled major element data for plagiogranite suites from diverse tectonic settings and ages, were unable to distinguish between residual and anatectic plagiorhyolites, particularly those with >70% SiO_2, on the basis of major elements. The problems are illustrated by major element mass balance calculations, based on average representative microprobe analyses of Water Island augite and plagioclase phenocrysts (Lidiak, unpublished data), together with likely titanomagnetie (Smith et al., 2003) and olivine compositions (Table 3, see Appendix). Models reveal that major element compositions similar to Water Island plagiorhyolites (such as sample 23 in Table 1) can be produced, with minimal residuals, by removal of observed phenocrysts from representative basalts (such as sample 42). However, the models, which produce a maximum of 10-20% felsic residua, are inconsistent with observed frequency distribution in the Water Island Fm, where plagiorhyolite is dominant. Also, fractional crystallization cannot account for the absence of andesite from the Water Island Fm and many analogous Cenozoic bimodal associations (cf., Aleutians, Tsvetlov, 1991).

Incompatible trace element fractional crystallization models

Development of Samail-type residual plagiogranite suites by advanced fractional crystallization of basaltic melts is evaluated utilizing trondhjemite lavas from the pre-arc MORB assemblage (Lower Cajul Basalt, Jolly et al., 1998b) in southwestern Puerto Rico (Fig. 1; Schellekens et al., 1990). Normalized patterns of tholeiite basalts and associated amphibolites are subparallel to average N-MORB, and together the patterns form an essentially flat field except for leftward depletion with respect to Sm of more incompatible components, particularly La, Nb, and Th. The rocks have a wide range of Yb_N, from between 0.9 and 20 in amphibolites (Fig. 8A and 9B), 15-30 in tholeiites, and a maximum between 60 and 80 in trondhjemite end-members. Evolved trondhjemites, with SiO_2 between 65 and 70%, have more elevated normalized patterns and deep negative Nb-, Eu-, and Ti-anomalies, reflecting extensive low pressure fractional crystallization of plagioclase plus ilmenite. A likely fractional crystallization origin for the trondhjemites is confirmed by trace element fractional crystallization models (Fig. 8C), evolved liquid residua from which reproduce key geochemical features of the rocks, including significant incompatible element enrichment and deep negative normalized Ti- and Nb-anomalies. Conversely, the models produce normalized patterns (Yb_N >10) that are consistently more elevated than Water Island plagiorhyolites (Yb_N <10).

Low-pressure crustal anatexic (Canyon Mountain-type) models

Low-HFSE plagiorhyolites (VIWI-4) are subdivided in Figs. 9A and 9B into two types. One set of three samples has relatively flat patterns and small negative Ce-anomalies (VIWI-4a, Fig. 1A); another set of two samples has comparatively deep negative Ce-anomalies (VIWI-4b, Fig. 8B). The envelope of normalized low-HFSE plagiorhyolites patterns is compared with basalts (VIWI-1) in Fig. 9C. Although the two end-members have similar negative Ce-anomalies, basalts have steep leftward decreases in normalized LREE (Fig. 8C). Since fractional crystallization of plagioclase plus quartz produces progressive LREE depletion, the more LREE-enriched normalized slopes of plagiorhyolites compared with basalts are inconsistent with a co-magmatic origin.

High-HFSE plagiorhyolites (VIWI-5), like their low-HFSE counterparts, have relatively flat normalized MREE – HREE segments. The rocks are subdivided on the basis of LREE-MREE segments into two types, one with slightly enriched (VIWI-5a in Fig. 9D) and another with slightly depleted LREE spectra with respect to Sm (VIWI-5b in Fig. 9E). As in low-HFSE varieties, the contrasting patterns indicate high-HFSE plagiorhyolites represent a variety of magma types, produced by melting in a range of sources with slightly different compositions. A similar conclusion arises from phenocryst distribution in high-HFSE plagiorhyolites. Plagioclase-quartz porphyries (denoted b in Figs. 3B, 9), representing the most silica enriched end-members, have slightly enriched LREE segments with high La compared with relatively phenocryst-poor low-HFSE plagiorhyolites, inconsistent with an ori-

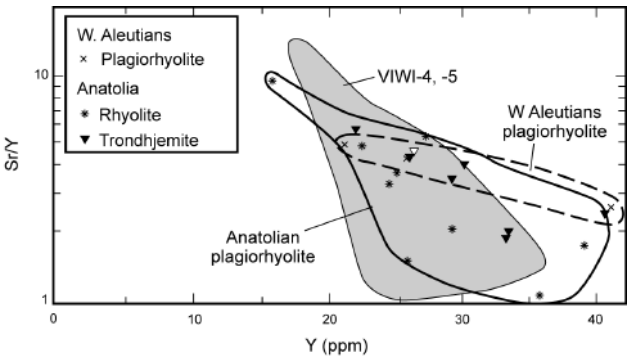

FIGURE 7 | **Covariation of Sr/Y with Y in selected Cenozoic arc basalts compared with the field of Water Island plaiorhyolites (VIWI-4 and -5), see text for references.**

gin through fractional crystallization of the observed plagioclase plus quartz phenocryst assemblage. The compositional variations in Water Island plagiorhyolite compared with basalts also excludes separation of an immiscible liquid (Dixon and Rutherford, 1979) as a potential mechanism for production of plagiorhyolite.

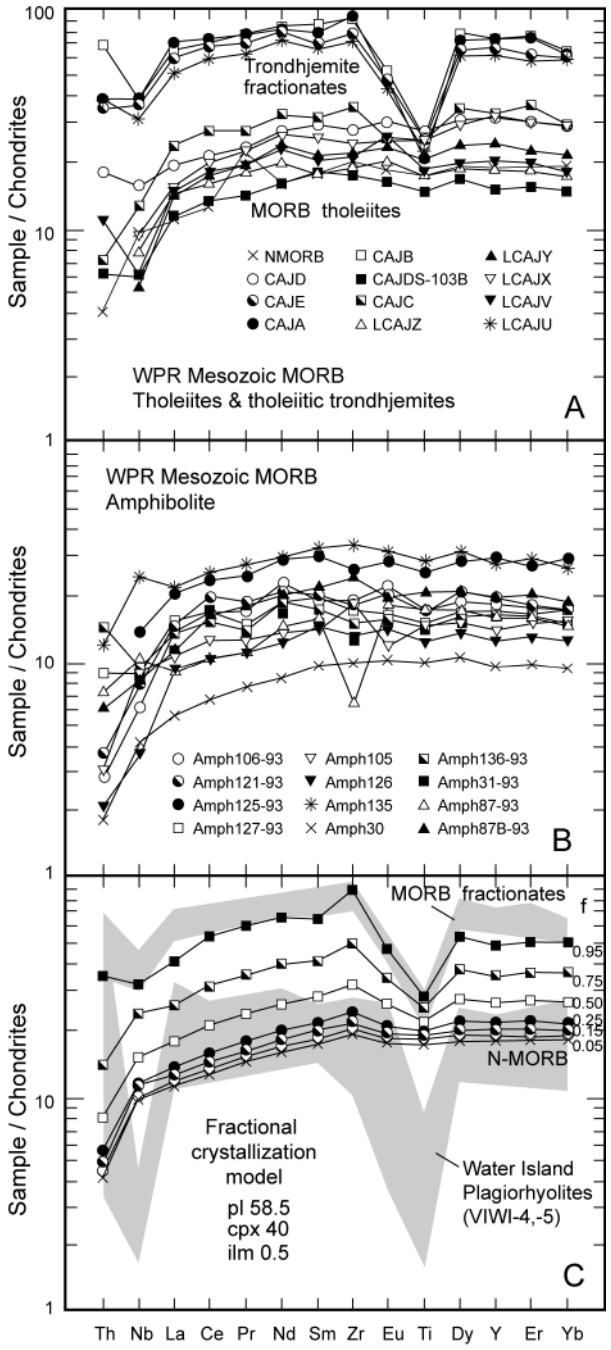

FIGURE 8 | **A) and B) Chondrite normalized patterns for A) MORB tholeiites and trondhjemitic fractionates from the Cajul Fm and B) Las Palmas Amphibolites, both from the pre-arc Sierra Bermeja Complex in southwest Puerto Rico (Table 2), representing rock types available in sub-arc oceanic crust. C) Fractional crystallization model (pl 58.5%, cpx 40, ilm 0.5) for an N-MORB composition (f, proportion crystallized). Selection of partition coefficients is discussed in text. Calculated patterns of more evolved fractionates resemble tholeiitic trondhjemite fractionates from the Puerto Rican pre-arc MORB suite, but are much more elevated than Water Island plagiorhyolites.**

Canyon Mountain-type crustal anatexis models, calculated utilizing a modification of the Shaw (1970) equation for equilibrium modal batch melting, produce more appropriate results. Partial fusion is evaluated in Fig. 10 for two different types of altered basaltic crust, amphibole gabbro and amphibolite. Crustal melting induced by introduction of mantle-derived melts is most likely to occur in the lower crust, where mafic gabbros and associated accumulates predominate (see for example, Floyd et al., 1998). Accordingly, an incompatible element depleted amphibolite from the basement complex in western Puerto Rico was selected as starting composition (sample AMPH30, Table 2 and Fig. 8B). When cast as an amphibole gabbro source (model 1), consisting of a 40:44:15:1 mixture of augite, plagioclase, hornblende and ilmenite, melting of this sample produces slightly depleted chondrite-normalized REE patterns that, at relatively high degrees of melting (25-50%), closely resemble Water Island plagiorhyolites (VIWI-5a). The patterns also have similar negative Eu anomalies, reflecting residual feldspar, deep negative Nb- and Ti-anomalies, consistent with fractional crystallization of Ti-bearing oxide phases, and slight positive Zr-anomalies (Fig. 9E). An amphibolite source (model 2), representing a more highly altered gabbro consisting of a 55:44:1 mixture containing hornblende, plagioclase and ilmenite, produces melts with slightly enriched normalized LREE slopes with respect to Sm at relatively low degrees of melting (15-25%), matching appropriate high-HFSE plagiorhyolites (VIWI-5b, Fig. 8F). Both models indicate melts similar to Water Island plagiorhyolites can be generated by melting in amphibole-bearing crustal materials at low pressures, producing plagioclase-rich residua.

Results for key incompatible trace element ratio-pairs.

Melting models are further evaluated in Figs. 11 and 12 utilizing selected trace element ratio pairs, which have the advantage of minimizing the effects of fractional crystallization. These include 1) Nb/Zr and the adjacent pair La/Nb, reflecting mantle composition and the relative magnitude of negative Nb-anomalies, respectively, 2) La/Sm and Sm/Yb, representing slopes of normalized LREE-MREE and MREE-HREE segments, and 3) Sm/Yb and the adjacent pair Zr/Sm, reflecting magnitude of Zr/Sm anomalies relative to slopes of normalized MREE-HREE segments. Included in the diagrams are calculated mixing curves (Jolly et al., this volume) representing compositions of melts (f = 0.25) from selected peridotite sources (FMM, RMM1, RMM2, and

RMM5) contaminated by pelagic sediments, and trajectories (bold lines) and melt proportions (0.05, 0.15, 0.25, 0.50) predicted (Fig. 10) by low-pressure melting models 1 (amphibole gabbro) and 2 (amphibolite).

La/Nb–Nb/Zr

The three major basaltic subunits (VIWI-1, -3) are intermediate between the mantle trend and pelagic sediment (AKPS) on La/Nb-Nb/Zr plots, where the rocks concentrate along the RMM2-average AKPS mixing line (Fig. 11). Low La/Nb in MORB-like basalts (VIWI-3) are consistent with a lower degree of melting (~15% compared to 25% for VIWI-1. see also Fig. 4D), and with a combination of decompression- and flux-related melting processes. The field of Water Island boninitic basalts (VIWI-1) form a vertical field that overlaps calculated mixing curves for source-sediment mixtures (f = 0.25, Jolly et al., this volume). The absence of significant negative normalized Ce-anomalies in low Nb/Zr basalts is consistent with low sediment proportions or with significant crustal contamination. Conversely, mixing lines indicate samples with higher Nb/Zr contain from <0.5 to 1.5% pelagic sediment (average Atlantic Cretaceous pelagic sediment (AKPS, Jolly et al., this volume). The presence of small negative Ce-anomalies in most Water Island basalts is consistent with the presence of a significant sediment component. Melting trajectories for models 1 and 2 both track across the field of high-HFSE plagiorhyolite, consistent with fusion at crustal pressures. The high-HFSE group (VIWI-5) is approximately aligned along calculated melt trajectories, indicating negligible sediment, whereas low-HFSE types (VIWI-4) have slightly higher Nb/Zr, consistent with a small sediment contribution.

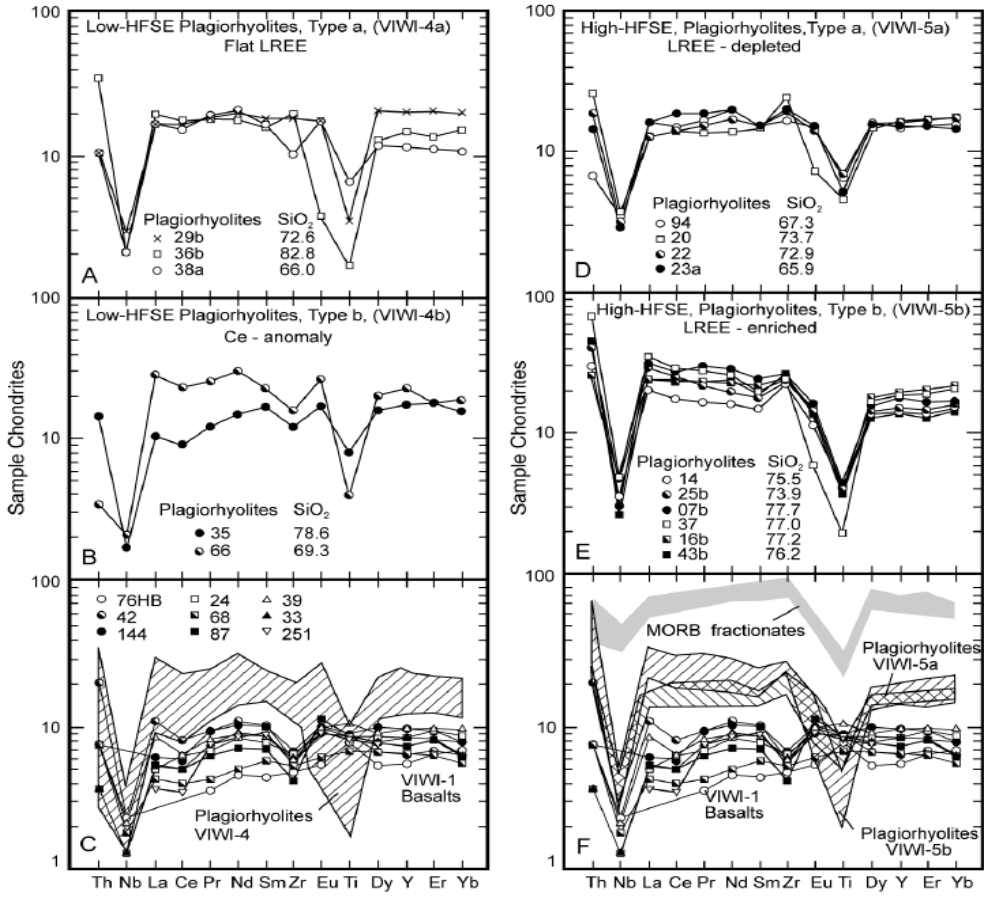

FIGURE 9 | **Comparison of chondrite normalized incompatible trace element patterns from Water Island basalts and plagiorhyolites; normalization values are from Sun and McDonough (1989). SiO_2 content (volatile free) of the rocks is indicated; letter a following plagioclase sample numbers indicates plagioclase porphyries; b indicates plagioclase-quarts porphyries, unmarked samples are phenocryst-poor. A) through C) Subdivision of low-HFSE plagiorhyolites into types with A) flat-LREE segments (VIWI-4a) and B) significant negative Ce-anomalies (VIWI-4b), and comparison of the low-HFSE plagiorhyolite field with boninitic basalts (VIWI-1). Although both groups have significant negative Ce-anomalies, the basalt suite has moderate LREE depletion, whereas plagiorhyolites have predominantly flat patterns. D) through F) Subdivision of high-HFSE plagiorhyolites into slightly depleted (VIWI-5a) and enriched (VIWI-5b) types based on configuration of normalized LREE segments. Included in C for comparison is the field of evolved trondhjemitic tholeiites from southwest Puerto Rico (from Fig. 8C).**

La/Sm– and Zr/Sm–Sm/Yb

Relations between ratio pairs involving REE elements confirm interpretations drawn from La/Nb-Nb/Zr. For instance, high-HFSE plagiorhyolites (VIWI-5, Figs. 12C and 12F) are aligned along or closely associated with the mantle trend (Figs. 12A and 12D) in La/Sm–Sm/Yb and Zr/Sm–Sm/Yb diagrams, consistent with melting in a source composed of sediment-poor oceanic crust. This interpretation is verified by melting trajectories for models 1 and 2 (Figs. 10C and 10D), which reflect up to 50% fusion of amphibole gabbro and amphibolite. In comparison, low-HFSE plagiorhyolites (VIWI-4) have anomalously low Zr/Sm, indicating the presence of significant sediment. Basalts (VIWI-1) have low La/Sm and overlap the MORB field, indicating a minimal crustal component, but a significant pelagic sediment component. Sm/Yb is slightly displaced to the right in these diagrams, due to fractional crystallizations (fc) of clinopyroxene (see fc vectors in Figs. 12A and 12D). As a result, the plots produce slightly higher estimates of sediment proportions, ranging from approximately 0.5 to 2%, compared with values derived from La/Nb–Nb/Zr, which has compensating plagioclase and clinopyroxene fractional crystallization vectors (Fig.11A). Anomalously low Zr/Sm in sheeted dikes (VIWI-2, Fig. 12E) are consistent with (1) a highly depleted source composition compared with a MORB source, or (2) incorporation of a unique, relatively low-Zr sediment component.

Ce-anomalies $(Ce/Ce^*)_N$

Normalized relations between measured and expected Ce (Ce* = [La minus Pr]/2 + La)$_N$ are compared with SiO_2 in Fig. 13. It is generally inferred that negative Ce/Ce* anomalies in island arc basalts are produced by Ce-depletion in the sediment component (Ben-Othman et al., 1989; Plank and Langmuir, 1998). This interpretation is consistent with measured compositions of Atlantic Mesozoic pelagic sediment (AKPS; see Jolly et al., this volume), which has average $(Ce/Ce^*)_N$ of 0.88 (range from 0.72 to 0.98). In comparison, pre-arc Mesozoic MORB (Table 2), reflecting the approximate compositional range of source compositions in the northeast Antilles, has a higher average value of 1.08 (range from 0.98 to 1.18). Water Island basalt subunits have wide ranges of $(Ce/Ce^*)_N$. Water Island boninitic basalts (VIWI-1 and -2) have values ranging from approximately

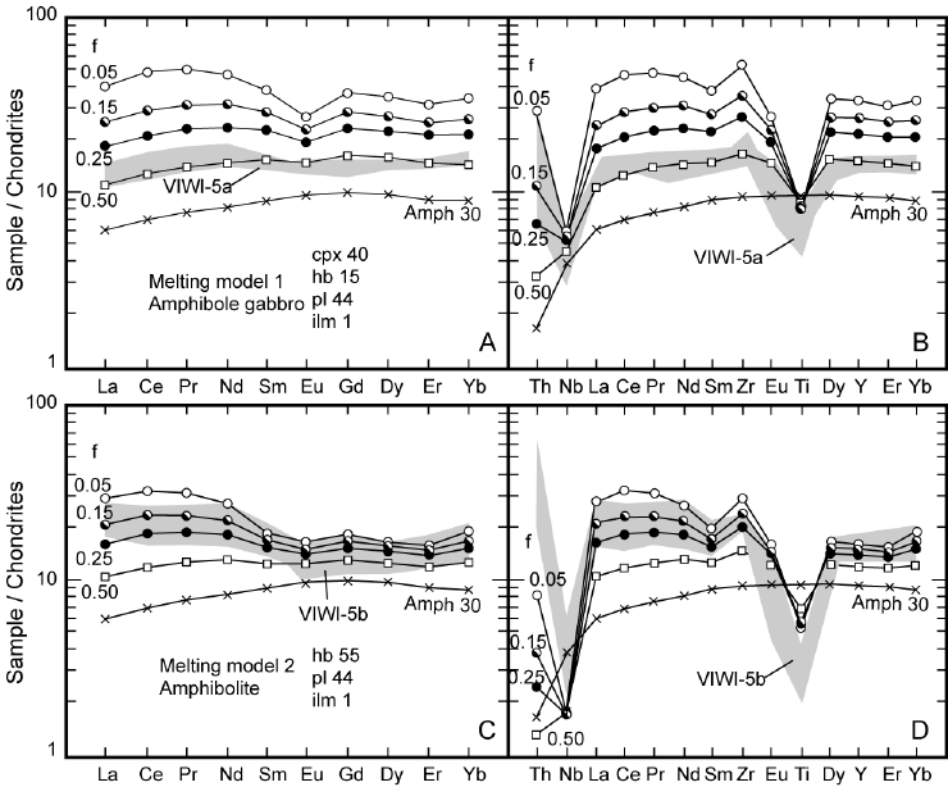

FIGURE 10 | **Low-pressure partial melting models in amphibole-bearing oceanic crust with composition of low-REE amphibolite sample AMPH-30 (Table 2) from the pre-arc basement MORB suite, western Puerto Rico (see Fig. 4C). Subdivision of plagiorhyolites is from Fig. 9. Symbols as follows: cpx: clinopyroxene; hb: hornblende; pl: plagioclase; ilm: ilmenite. A) and B) Melting model 1 - Chondrite-normalized patterns representing low pressure crustal fusion (f = melting proportion) in amphibole gabbro (cpx 40 %, hb 15, pl 44, ilm 1); the field of plagiorhyolite VIWI5a closely resembles calculated fraction patterns between 25 and 50% melting. C) and D) Melting model 2 - calculated patterns for 15 to 25% fusion in amphibolite (hb 55, pl 44, ilm, 1) resemble field of plagiorhyolite VIWI5b.**

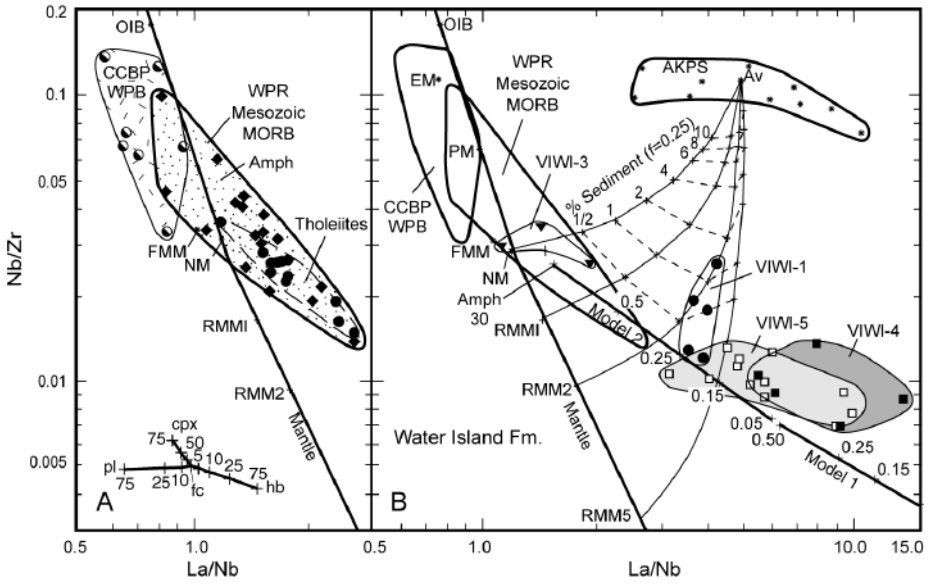

FIGURE 11 | **La/Nb-Nb/Zr (relative magnitude of Nb-anomalies compared to degree of incompatible enrichment); mantle components include FMM, fertile MORB mantle; RMM2, residual mantle after removal of 2% melt; RMM5 (Pearce and Parkinson, 1993); OIB, ocean island basalt; EM, E-MORB; PM, primitive mantle, and NM, N-MORB are from Sun and McDonough (1989). Mixing lines (f = 0.25) between Atlantic Mesozoic pelagic sediment (AKPS) and various source compositions are from Jolly et al. (this volume). Fractional crystallization trends to 75% solid for pl, hb, and cpx are indicated by vectors. AKPS represent Atlantic Creaceous pelagic sediment (Jolly et al., this volume). A) Pre-arc Mesozoic MORB from Puerto Rico (Table 2), including representative compositions of Caribbean Cretaceous Plateau Basalts (CCPB) from the central Caribbean (Kerr et al., 1999, 2002; Hauff et al., 2000). B) Water Island lava subgroups; symbols as in Figs. 3B and 3D. Water Island MORB-like basalts with low La/Nb cluster near the WPR Mesozoic MORB field (symbols as in Fig. 4C); boninitic Water Island basalts (VIWI-1) concentrate along calculated mixing lines for melting in peridotite sources with RMM2-5 compositions (Pearce and Parkinson, 1993), whereas Water Island plagiorhyolites have elevated La/Nb. Plagiorhyolite fields are compared to calculated melting models 1 and 2 (Fig. 10) for fusion in amphibole gabbro and amphibolite, respectively. Plagiorhyolites lie along or near calculated melting tracks; low-HFSE types are slightly more elevated, consistent with a significant pelagic sediment component.**

0.65 to 1.5, but most samples are concentrated within a tight field averaging 0.78, indicating the presence of a significant sediment component. Three samples, designated WIVI-1' in Fig. 13B, have near expected values of $(Ce/Ce^*)_N$, reflecting limited sediment content and possibly due to crustal contamination. MORB-like basalts (VIWI-3) have a narrower range (from approximately 0.85 to over 1.15, indicating variable but predominantly low sediment proportions. Since Nb-Yb abundances are consistent with relatively low degrees (5-15%) of melting (Fig. 4D), it is inferred MORB-like basalts represent samples of melts generated predominantly by decompression-related melting in the back arc region of the mantle wedge, where proportions of contaminating sediment are more limited (Hochstaedter et al., 1990). Low La/Nb-Nb/Zr (Fig. 11B) in MORB-like basalts indicates a minimal crustal component.

$(Ce/Ce^*)_N$ values in Water Island plagiorhyolites, ranging between 0.8 and 1.1, are similar to MORB, but higher than most boninitic basalts (VIWI-1). The two distinctive plagiorhyolite subunits have partly overlapping fields (Fig. 13B), but high-HFSE types (VIWI-5) have an average $(Ce/Ce^*)_N$ of 0.98, slightly above the expected value, indicating a negligible sediment component, whereas low-HFSE types (VIWI-4) have a lower average of 0.92, indicating the presence of significant sediment. The absence of intermediate members in the Water Island Fm is inconsistent with significant hybridization of mafic and felsic end-members of the Water Island Fm. Instead, the distribution of compositions indicates low-HFSE plagiorhyolites incorporated significant proportions of re-melted gabbro of island arc origin. Possible re-melted sources include (1) gabbroic segregations, such as feeder veins, dikes, and sills intimately associated with the sub-arc oceanic crust, and (2) sub-crustally underplated, still hot, layered plutonic intrusive bodies produced by solidification of earlier boninitic basalts.

Summary of petrogenetic constraints on the Water Island Fm

Petrogenetic evidence from Water Island basaltic subunits, summarized in Table 4a (see Appendix) is consistent with the following interpretations: (1) Low Nb and Yb abundances (following correction for olivine fractional crystallization during elevation to crustal levels), intermediate TiO_2 (~0.5%), and Cr-Yb relations indicate boninitic basalts (VIWI-1 and -2) were generated by melting in a moderately incompatible element depleted mantle source (RMM2-5). Compositions of MORB-like basalts (VIWI-3) are consistent with lower degrees of melting in a similar mantle source. Degree of melting

averaged between 15 and 25% for boninitic basalts (VIWI-1), but was consistently lower for MORB-like types (5-15%). (2) Estimates of pelagic sediment proportions, derived from La/Nb-Nb/Zr, range from <0.5 to 1.5% in boninitic basalts (VIWI-1); Zr/Sm- and La/Sm-Sm/Yb produce similar but slightly higher estimates. Low $(Ce/Ce^*)_N$ in most basalts is also consistent with the presence of a significant sediment component. (3) Low La/Nb in Water Island basalts compared with plagiorhyolites indicates incorporation of a negligible crustal component. (4) Major and trace element compositions of plagiorhyolite subunits, characterized by low Al_2O_3, Sr, Sr/Y<10, and relatively flat normalized REE spectra, indicate melts were generated in a hydrous environment at crustal pressures in equilibrium with plagioclase. This inference is consistent with low TiO_2 and Nb, which are retained by Ti-bearing oxide minerals during hydrous melting. (5) $(Ce/Ce^*)_N$, Zr/Sm-Sm/Yb, and La/Nb-Nb/Zr relations indicate low-HFSE plagiorhyolites (VIWI-4) have a significant sediment component, whereas high-HFSE types (VIWI-5) have negligible sediment. Absence of intermediate members from the Water Island Fm indicates sediment in low-HFSE plagiorhyolites was contributed by remelted arc-related crustal gabbros rather than by magma mixing. (6) Low-pressure melting models involving moderate degrees of fusion (25-50%) in amphibole gabbro are consistent with slightly depleted normalized LREE slopes (similar to VIWI-5a; Fig. 9D). Slightly enriched LREE

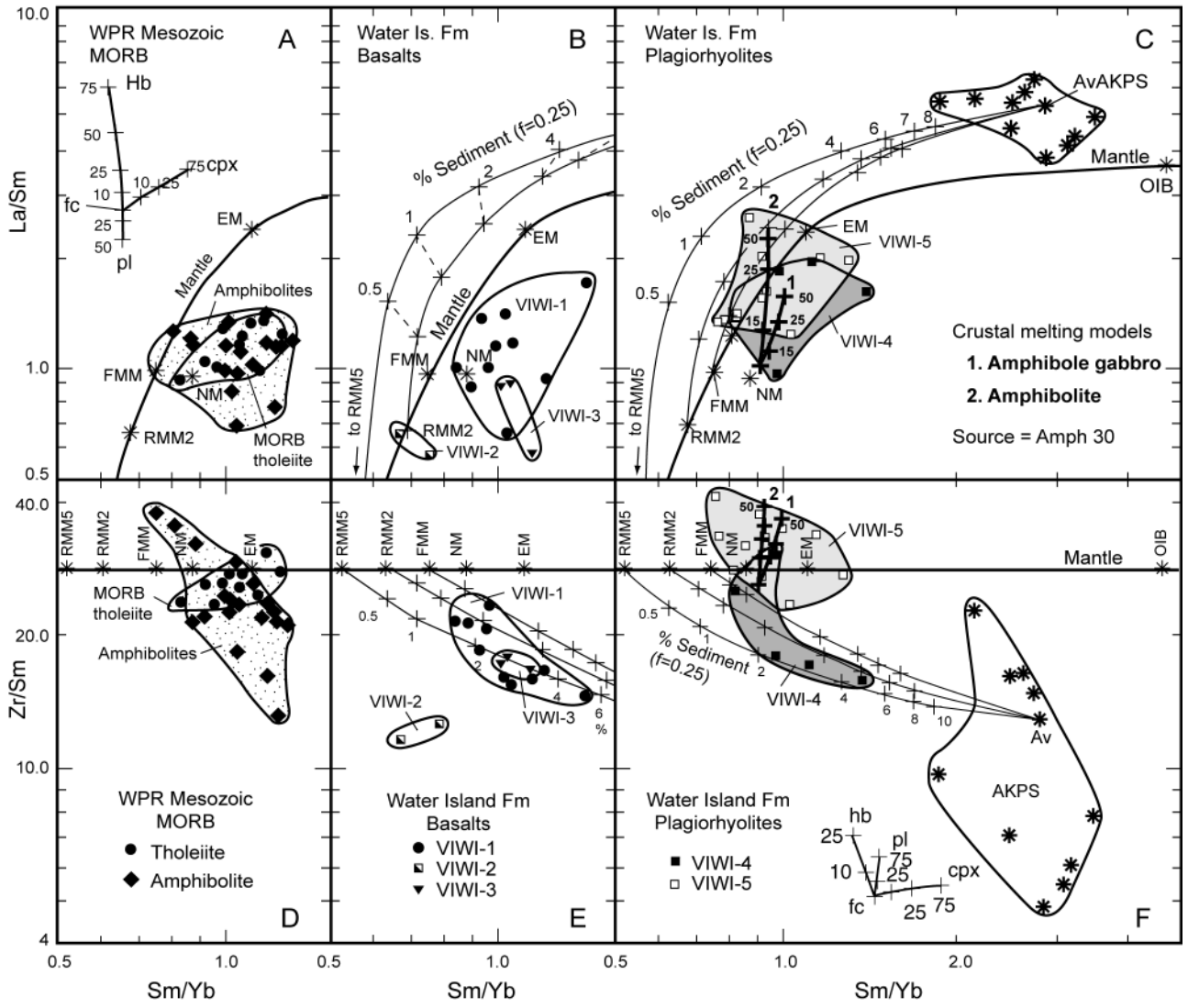

FIGURE 12 | **Sm/Yb-La/Sm (comparison of MREE-HREE and LREE-MREE segments) and Sm/Yb-Zr/Sm (HFSE-MREE relations compared to MREE-HREE). Unit fields and symbols, mixing lines, fractional crystallization vectors, mantle components, and pelagic sediment field as in Fig. 11. Bold lines and symbols represent calculated crustal melting models 1 and 2, in amphibole gabbro and amphibolite, respectively; 15, 25, and 50 represent degree of melting. Melting models are restricted to the field of high-HFSE plagiorhyolite (VIWI-5), consistent with an origin by fusion in amphibole-bearing MORB-like gabbro. Low-HFSE plagiorhyolites (VIWI-4) have anomalously low Zr/Sm, consistent with contamination by sediment-bearing basalt melt.**

slopes (as in VIWI-5b, Fig. 9E) are consistent with lower degrees of fusion (5-25%) in amphibolite.

Crustal heating alone is insufficient for generating voluminous melt from oceanic crust, particularly in refractory gabbroic accumulates comprising lower parts of oceanic crustal sequences (Floyd et al., 1998; Koepke et al., 2004). Jolly et al. (this volume) suggested that low sediment contents in Virgin Island volcanic rocks, compared with samples from central Puerto Rico, are consistent with subduction of the still hot proto-Atlantic ridge system. If so, then high heat flow in the Virgin Islands was generated within the subducting plate. In addition, copious quantities of aqueous fluid, such as are stored in pargasitic amphibolite, serpentinite, and other hydrous alteration products, are also required to flux the melting process (Koepke et al., 2004). Judging from exposed ophiolite sequences, however, the volume of fluid available in the lower gabbroic oceanic crust is severely limited (Floyd, et a., 1998). Instead, the most likely sources of fluid flux in an island arc tectonic setting are hydrothermal processes associated with crustal underplating by arc-related basalt magmas (Smith et al., 2003; cf. Tsvetlov, 1991). Accordingly, it is inferred crustal melting was largely confined to hydrothermally altered parts of the lower crust, especially in the vicinity of stratigraphic discontinuities, shear zones, fractures, veins and other relatively permeable channelways. Widespread hydrothermal alteration of Water Island plagiorhyolites (Rankin, 2002) is consistent with this interpretation.

Plagiorhyholite sequences in Cenozoic arcs (cf. Aleutians, Tsvetlov, 1991; Kermadecs, Smith et al., 2003) are normally produced following an interval of basalt volcanism during which the sub-arc crust is progressively heated in response to both continuous transmission of melts to the surface and crustal underplating by arc-related gabbro. Consequently, it inferred a considerable thickness of older basalt underlies the predominantly plagiorhyolite-bearing Water Island strata exposed in the Virgin Islands.

CONCLUSIONS

Virgin Island lavas from the bimodal Water Island Fm (Late Aptian to Early Aptian, i. e. 115 Ma; Rankin, 2002) consist predominantly of plagiorhyolite (80%; SiO_2 = 65 to 85% on a volatile-free basis) interlayered

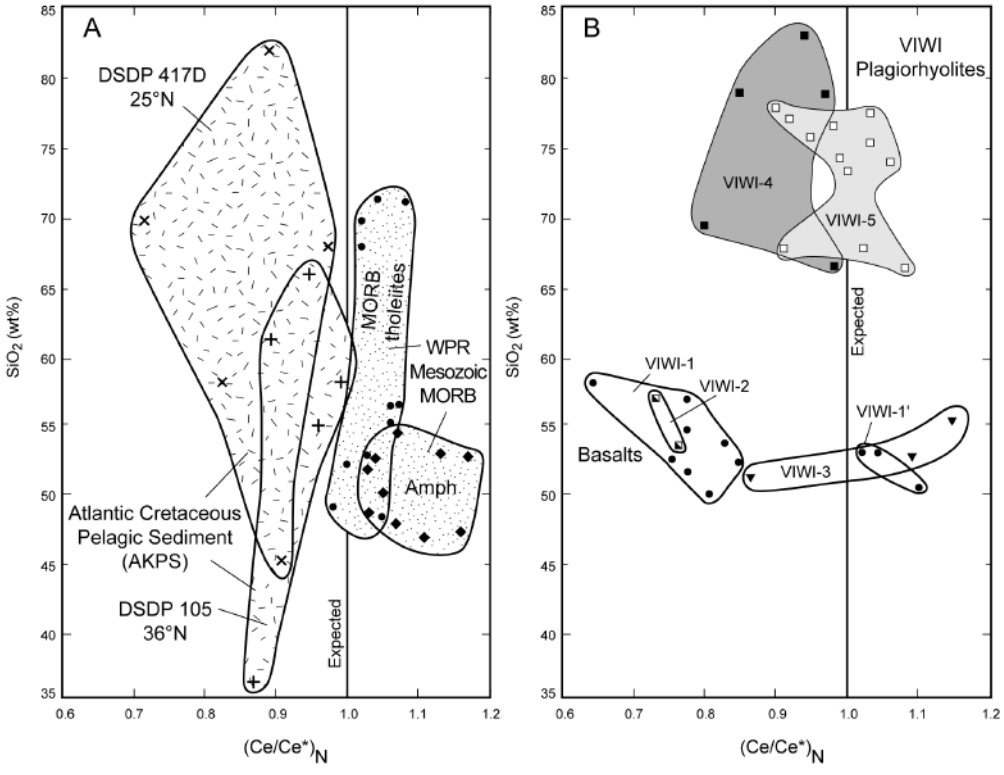

FIGURE 13 | **$(Ce/Ce^*)_N$. A) Ce-anomalies in Atlantic Cretaceous pelagic sediment (AKPS; Jolly et al., this volume) and pre-arc MORB tholeiites and amphibolites (Amph) from western Puerto Rico (WPR; Table 2); DSDP105 and DSDP417D represent sediment compositions in drill cores from the deep-sea drilling program taken at indicated localities. B) Ce-anomalies in Water Island basalts and plagiorhyolites; symbols are identified in Figs. 3 and 4.**

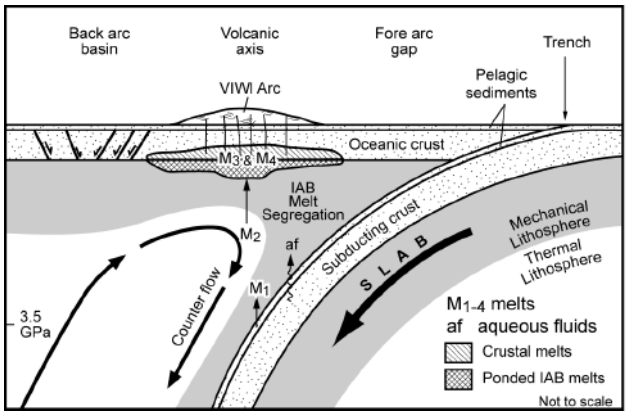

FIGURE 14 | **Schematic tectonic model (not to scale) of subduction setting of the Water Island Fm. Geographic subdivisions are from Jarrard (1986), mantle configuration is from Peacock (1993), and back-arc convection patterns are from summary of Pearce and Parkinson (1993). Aqueous fluids emanating from the slab are identified as af; possible melt fractions include M-1, sediment melt (Nicholls et al., 1994); M-2, spinel peridotite melt; M3, basalt-contaminated crustal melt; M-4, crustal melt with a limited sediment component.**

with subordinate basaltic rocks (20%; SiO_2 ? 49 to 58). Basalts are characterized by moderate TiO_2 content (average 0.5%, Fig. 4B) resembling borderline intermediate-Ti boninitic basalts in the classification of Bédard (1999). The basalts also have low Yb (Fig. 4C and D), MORB-like HFSE (Fig. 4D), and slightly lower average LREE abundances (La < 1.5 ppm, Fig. 3C) than N-MORB. These features are consistent with a mantle source composition that was significantly depleted in incompatible elements relative to an N- MORB-type source, presumably due to (1) MORB-melting processes during original plate formation or (2) low-degree decompression fusion in the back arc region (Speigelman and McKenzie, 1985). In comparison, temporally correlated Albian volcanic strata in central Puerto Rico have higher TiO_2, ranging from 0.6 to 1.1% (Fig. 4B), similar to the most Cenozoic island arc basalts (Pearce and Parkinson, 1993). Water Island basalts have relatively elevated Nb/Zr compared with MORB-type sources. In the absence of a recognizable OIB-type component these features indicate basalts contain a small pelagic sediment component (0.5 to 1.5%).

Plagiorhyolites in the Water Island Fm have low REE, Al_2O_3, and Sr/Y<10, similar to plagiorhyolite end-members of Cenozoic bimodal arc suites (western Aleutians, Izu-Bonin, the Kermadecs). Experimental and incompatible trace element evidence and theoretical melting models are all consistent with an origin of plagiorhyolite through fusion of hydrothermally altered oceanic crust within the stability range of plagioclase. Accordingly, the predominance of felsic end-members in Water Island strata indicates availability of a long-term source of heat and aqueous fluids at depth, and implies early mantle-derived island arc melts were underplated along the sub-arc crust-mantle boundary. Moreover, truncation of the basalt fractional crystallization series at SiO_2 = 58% indicates basalt crystal fractionates were eventually largely displaced from the crustal melt conduit system by more buoyant plagiorhyolite liquids and became trapped instead within permanent sub-crustal magma chambers. A small sediment component in certain plagiorhyolite samples (low-HFSE subunit WIVI-4), together with the absence of intermediate andesitic members from the Water Island Fm, is consistent with incorporation of re-melted hydrothermally altered, arc-related amphibole-bearing gabbro intimately associated with the sub-arc crust or within underplated layered gabbroic plutons. High heat flow in the Virgins Islands probably resulted from subduction of the still hot proto-Atlantic ridge system (see Jolly et al., this volume).

ACKNOWLEDGEMENTS

This paper is a contribution to the IGCP Project 433. The authors gratefully acknowledge reviews of the original manuscript by Mark Feigenson, J. F. Lewis, D. W. Rankin, and J. J. W. Rogers. Doug Rankin kindly shared his insights into the geology of St. John, VI. Graphics were prepared by Mike Lozon (Department of Geological Sciences at Brock University). Financial assistance for this project is provided by the National Science and Engineering Research Council of Canada (NSERC), and by IGCP Project 433 on Tectonics of the Caribbean Plate Boundary.

REFERENCES

Alabaster, T., Pearce, J.A., Malpas, J., 1982. The volcanic stratigraphy and petrogenesis of the Oman ophiolite. Contributions to Mineralogy and Petrology, 81, 168-183.

Barbieri, M., Caggianelli, A., Di Florio, M.R., Lorenzoni, S., 1994. Plagiogranites and gabbroic rocks from the Mingora ophiolite mélange, Swat Valley, NW Frontier Province, Pakistan. Mineralogical Magazine, 58, 553-566.

Baker, D.R., Eggler, D. H., 1987. Compositions of anhydrous and hydrous melts coexisting with plagioclase, augite, and olivine or low-Ca pyroxene from 1 atm to 8 kbar: application to the Aleutian volcanic center of Atka. American Mineralogist, 72, 12-28.

Barker, F., 1979, Trondhjemites, Dacites, and Related Rocks. Amsterdam, Elsevier, 659pp.

Beard, J.S., 1995. Experimental, geological, and geochemical constraints on the origins of low-K silicic magmas in oceanic arcs. Journal of Geophysical Research, 100, 15593-15600.

Beard, J.S., Lofgren, G.E., 1991. Dehydration melting and water-saturated melting of basaltic and andesitic greenstones

and amphibolites at 1,3, and 6.9 kb. Journal of Petrology, 32, 365-401.

Bédard, J.H., 1999. Petrogenesis of boninites from the Betts Cove Ophiolite, Newfoundlandl, Canada: Identification of subducted source components. Journal of Petrology, 40, 1853-1889.

Ben-Othman, D., White, W., Patchett, J., 1989. Geochemistry of marine sediments, island arc magma genesis, and crust-mantle recycling. Earth and Planetary Science Letters, 94, 1-21.

Burke, K., 1988. Tectonic evolution of the Caribbean. Annual Reviews of Earth and Planetary Sciences, 16, 201-30.

Carmichael, I.S.E., 1964. The petrology of Thingmuli in eastern Iceland. Journal of Petrology, 5, 434-460.

Casey, J.F., 1997. Comparison of major- and trace element geochemistry of abyssal peridotites and mafic plutonic rocks with basalts from the MARK region of the Mid-Atlantic Ridge. Procedings of ODP Science Results, 153, College Station TX, 181-241.

Coleman, R.G., Donato, M.M., 1979. Oceanic plagiogranite revisited. In: Barker, F. (ed.). Trondhjemites, dacites, and related rocks. Amsterdam-Oxford-New York, Elsevier, 149-167.

Coleman, R.G., Peterman, Z., 1975. Oceanic plagiogranite. Journal of Geophysical Research, 80, 1099-1108.

Cox, D.P., Marvin, R.F., McGonigle, J.W., McIntyre, D.H., Rogers, C.I., 1977. Potassium-argon geochemistry of some metamorphic, igneous, and hydrothermal events in Puerto Rico and the Virgin Islands. United States Geological Survey Journal of Research, 5, 689-703.

Crawford, A.J., 1989. Boninites and Related Rocks. London, Unwin Hyman ed., 279 pp.

Defant, M.J., Drummond, M., 1990. Derivation of some modern arc magmas by melting of young subducted lithosphere. Nature, 347, 662-665.

Defant, M.J., Richerson, P.M., De Boer, J.Z., Stewart, R.H., Maury, R.C., Bellon, H., Drummond, M.S., Feigenson, M.D., Jackson, T.E., 1991. Dacite genesis via both slab melting and differentiation: Petrogenesis of La Yeguada Volcanic Complex, Panama. Journal of Petrology, 32, 1101-1142.

Dick, H.J.B., Natland, J.H., Alt, J.C. et al., 2000. A long in situ section of the lower oceanic crust: results of ODP leg 176 drilling at the southwest Indian Ridge. Earth and Planetary Science Letters, 179, 31-51.

Dixon, S.J., Rutherford, M.J., 1979. Plagiogranites as late-stage immiscible liquids in ophiolite and mid-ocean ridge suites: An experimental study. Earth and Planetary Science Letters, 45, 45-60.

Donnelly, T.W., 1966. Geology of St. Thomas and St. John, U.S.Virgin Islands. In Hess, H. (ed.). Caribbean Geological Investigations. Geological Society of America Memoir, 98, 5-176.

Donnelly, T.W., 1989. Geologic history of the Caribbean and Central America. In Bally, A.W., Palmer, A.R. (eds.). Geology of North America-An Overview. Geological Society of America Special Paper, A, 299-321

Donnelly, T.W., Rogers, J.J.W., Pushkar, P., Armstrong, R.L., 1971. Chemical evolution of the igneous rocks of the eastern West Indies. In Donnelly, T.W. (ed). Caribbean Geophysical, Tectonic, and Petrologic Investigations. Geological Society of America Memoir, 130, 181-224.

Donnelly, T.W., Rogers, J.J.W., 1980. Igneous series in island arcs. Bulletin of Volcanlogy, 43, 347-382.

Donnelly, T.W., Beets, D., Carr, M.J., et al.,1990. History and tectonic setting of Caribbean magmatism. In Case, J.E. and Dengo, G. (eds.). Caribbean Region. Boulder, Colorado, Geological Society of America, H, 339-374.

Dosso, L., Bougault, H., Joron, J.-L., 1993. Geochemical morphology of the North Mid-Atlantic Ridge, 10-24º: Trace element-isotope complementarity. Earth and Planetary Science Letters, 120, 443-462.

Draper, G., Gutiérrez, G., Lewis, J.F., 1996. Thrust emplacement of the Hispañiola peridotite belt: orogenic expression of the mid-Cretaceous Caribbean arc polarity reversal. Geology, 24, 1143-1146.

Drummond, M.S., Defant, M.J., Kepezhinski, P.K., 1996. Petrogenesis of slab-derived trondhjemite-tonalite-dacite/adakite magmas. Transactions of the Royal Society of Edinborough: Earth Sciences, 87, 205-215.

Elthon, D., 1991. Geochemical evidence for formation of the Bay of Islands ophiolite above a subduction zone. Nature, 354, 140-145.

Ewart, A., Griffin, W.L., 1994. Application of proton-microprobe data to trace-element partitioning in volcanic rocks. Chemical Geology, 117, 251-284.

Flagler, P. A., Spray, J. G., 1991. Generation of plagiogranite by amphibolite anatexis in oceanic shear zones. Geology 19, 70-73.

Floyd, P.A., Yalinz, M.K., Goncuoglu, M.C., 1998. Geochemistry and petrogenesis of intrusive and extrusive ophiolite plagiogranites. Central Anatolian Crystalline Complex, Turkey. Lithos, 42, 225-241.

Frost, C.D., Schellekens, J.H., 1998. Rb-Sr and Sm-Nd isotopic characterization of Eocene volcanic rocks from Puerto Rico. Geophysical Research Letters, 18, 545-548.

Gerlach, D.C., Leeman, W.H., AveLallement, H.G., 1981. Petrology and geochemistry of plagiogranite in the Canyon Mountain Ophiolite, Oregon. Contributions to Mineralogy and Petrology, 77, 82-92.

Gill, J.B., 1981. Orogenic Andesites and Plate Tectonics. London, Springer, 390 pp.

Green, D.H., Pearson, N.J., 1987. An experimental study of Nb and Ta partitioning between Ti-rich minerals and silicate liquids at high pressure and temperature. Geochemica et Cosmochimia Acta 51, 55-62.

Harland, W.B., Cox, A.V., Llewellyn, P.G., Pickton, C.A.G., Smith, A.G., Walters, R., 1982. A Geologic Time Scale. Cambridge, UK, Cambridge University Press.

Hauff, F., Hoernle, K., Tilton, G., Graham, D.W., Kerr, A.C., 2000. Large volume recycling of oceanic lithosphere over short time scales: geochemical constraints from the

Caribbean Large Igneous Province. Earth and Planetary Science Letters, 174, 247-263.

Hébert, R., Constantin, M., Robinson, P.T., 1991. Primary mineralogy of Leg 118 gabbroic rocks and their place in the spectrum of oceanic mafic igneous rocks. Procedings of ODP, Science results, 118, Ocean Drilling Program, College Station, TX, 3-20.

Hekinian, R., 1971. Petrological and geochemical studies of spilites and associated rocks from St. John, U.S. Virgin Islands. Geological Society of America Bulletin, 82, 659-682.

Helsley, C.E., 1960. Geology of the British Virgin Islands. Doctoral Dissertation, NJ, Princeton University, 167 pp.

Hickey, R.L., Frey, F.A., 1982. Geochemical characteristics of bononite-series volcanics: implications for their source. Goechimica et Cosmochimica Acta, 46, 2009-2115.

Hirose, K., 1997. Melting experiments on lherzolite KLB-1 under hydrous conditions and generation of high-magnesian andesitic melts. Geology, 25, 42-44.

Hochstaedter, A.G., Gill, J.B., Morris, J.D., 1990. Volcanism in the Shmisu Rift, II. Subduction and non-subduction related components. Earth and Planetary Science Letters 100, 195-209.

Hopson, C.A., Coleman, R.G., Gregory, R.T., Pallister, J.S., Bailey, E.H., 1981. Geologic section through the Samail ophiolite and associated rocks along a Muscat-Ibra transect, southeastern Oman Mountains. Journal of Geophysical Research, 86, 2527-2544.

Horan, S., 1995. Geochemistry and tectonic significance of the Maimon-Amina Schists, Cordillera Central, Dominican Republic. M.Sc. Thesis, Gainsville, FL, University of Florida, 172 pp.

Housh, T.B., Luhr, J.F., 1991. Plagioclase-melt equilibria in hydrous systems. American Mineralogist, 76, 477-492.

Jafri, S. H., Charan, S.N, Govil, P. K., 1995. Plagiogranite from the Andaman ophiolite belt, Bay of Bengal, India. Journal of the Geological Society of London, 152, 681-687.

Jakeš, P., Gill, J.B., 1970. Rare earth elements and the island arc tholeiite series. Earth and Planetary Science Letters, 9, 17-28.

Jansma, P., Mattioli, G., Lopez, A., DeMets, C., Dixon, T.H., Mann, P., Calais, E., 2000. Neotectonics of Puerto Rico and the Virgin Islands, northeastern Caribbean, from GPS geodesy. Tectonics, 19, 1021-1037.

Jarrard, R.D., 1986. Relations among subduction parameters. Reviews of Geophysics, 24, 217-284,.

Jenner, G.A., Dunning, G.R., Malpas, J., Brown, M., Brace, T., 1991. Bay of Island and Little Port complexes revisited: Age, geochemical and isotope evidence confirm supra-subduction zone origin. Canadian Journal of Earth Sciences, 28, 1635-1652.

Juster, T.C., Grove, T.L., Perfit, M.R., 1989. Experimentsl constraints on the generation of Fe-Ti basalts, andesites, and rhyodacites at the Galapagos spreading center. Journal of Geophysical Research, 94, 9251-9274.

Jolly, W.T., Lidiak, E.G., Schelleckens, H.S., Santos, S., 1998a. Volcanism, tectonics, and stratigraphic correlations in Puerto Rico. In Lidiak, E.G., Larue, D.K. (eds.). Tectonics and Geochemistry of Northeast Caribbean. Geological Society of America Special Paper, 322, 1-34.

Jolly, W.T., Lidiak, E.G., Dickin, A.P., Wu, T-S., 1998b. Geochemical diversity of Mesozoic island arc tectonic blocks, eastern Puerto Rico. In Lidiak, E.G., Larue, D.K. (eds.). Tectonics and Geochemistry of the Northeastern Caribbean. Geological Society of America Special Paper, 322, 67-89.

Jolly, W.T., Lidiak, E.G., Dickin, A.P., 2001. Secular geochemistry of central Puerto Rican island arc lavas: constraints on Mesozoic tectonism in the Greater Antilles. Journal of Petrology, 42, 2197-2214.

Jolly, W.T., Lidiak, E.G., Dickin, A.P., 2002. Recycling in the Puerto Rican mantle wedge, Greater Antilles Island Arc. The Island Arc 11, 10-24.

Jolly, W.T., Lidiak, E.G., Dickin, A.P., 2006. Cretaceous to Mid-Eocene pelagic sediment budget in Puerto Rico and the Virgin Islands (northeastern Antilles Island Arc). Geologica Acta, 4, 35-62.

Kay, R.W., 1980. Volcanic arc magmas: implications of a melting-mixing model for element recycling in the crust-upper mantle system. Journal of Geology, 88, 497-522.

Kepezhinskas, P.K., Defant, M.J., Drummond, M.J., 1995. Na Metasomatism in the island-arc mantle by slab melt-peridotite interaction: evidence from mantle xenoliths in the North Kamchatka Arc. Journal of Petrology, 36, 1505-1527.

Kerr, A.C., Iturralde-Vinent, M.A., Saunders, A.D., Babbs, T.L., Tarney, J., 1999. A new plate tectonic model of the Caribbean: Implications from a geochemical reconnaisance of Cuban Mesozoic volcanic rocks. Geological Society of America Bulletin, 55, 1581-1599.

Kerr, A.C., Tarney, J., Kempton, P.D., Spaden, S., Nivia, A., Marriner, G.F., Duncan, R.A., 2002, Pervasive mantle plume head heterogeniety: Evidence from the late Cretaceous Caribbean-Columbina oceanic plateau. Journal of Geophysical Research, 107, 1029-2001.

Koepke, J., Feig, S., Snow, J., Freise, M., 2004. Petrogenesis of oceanic plagiogranites by partial melting of gabbro: an experimental study. Contributions to Mineralogy and Petrology, 146, 414-432.

La Maitre, R.W., 1989. A classification of Igneous Rocks and Glossary of Terms. Oxford, Blackwell, 193 pp.

Lapierre, H., Dupuis, V., Lepinay, B.M., Tardy, M., Ruiz, J., Maury, R.C., Hernandez, J., Loubert, M., 1997. Is the Lower Duarte Complex (Hispañiola) a remnant of the Caribbean plume generated oceanic plateau? Journal of Geology, 105, 111-120.

Lapierre, H., Dupuis, V., Lepinay, B.M., Bosch, D., Moni, P., Tardy, M., Maury, R. C., 1999. Late Jurassic oceanic crust and Upper Cretaceous Caribbean Plateau picritic basalts exposed in the Duarte igneous complex, Hispañiola. Journal of Geology, 107, 193-207.

Leat, P.T., Larter, R.D., 2003. Intra-oceanic subduction systems: introduction. Intra-ocanic subduction systems: Tectonic and magmatic processes. The Geological Society of London, 219, 1-18.

Leat, P.T., Smellie, J.L., 2003. Magmatism in the south Sandwish arc. The Geological Society of London, 219, 285-313.

Lebron, M.C., Perfit, M.R., 1994. Petrochemistry and tectonic significance of Cretaceous island arc rocks, Cordillera Oriental, Dominican Republic. Tectonophysics, 229, 60-100.

Lewis, J.F., Astacio, V.A., Espaillat, J., Jimenez, J., 2000. The occurrence of volcanogenic sulfide in the Maimon Formation, Dominican Republic: the Cerro Maimon, Loma Pesada and Loma Banbuito deposits. In: Sharlock, R., Barsch, R., Logan, A. (eds.). VMS Deposits of Latin America. Geological Society of Canada Special Publication, 228-249.

Lewis, J.F., Escuder Viruete, J., Hernaiz Huerta, P.P., Gutierrez, G., Draper, G., Pérez-Estaun, A., 2002. Subdivisión geoquímica del Arco Isla Circum-Caribe, Cordillera Central Dominicana: Implicaciones para la formación, acreción, y crecimiento cortical en un ambiente intraoceánico. Acta Geologica Hispanica, 37, 81-122.

Lewis, J.F., Hames, W.E., Draper, G., 1999. Late Jurassic oceanic crust and Upper Cretaceous Caribbean Plateu picritic basalts exposed in the Duarte Igneous Complex, Hispaniola: A discussion. Journal of Geology, 107, 235-235.

Lewis, J.F., Jiménez, J.G., 1991. Duarte Complex in the La Vega-Jarabacoa-Janico Area, Central Espaniola: Geological and geochemical features of the sea floor during early stages of arc evolution. Geological Society of America Special Paper, 262, 115-142.

Lidiak, E.G., Jolly, W.T., 1996. Circum-Caribbean granitoids: Characteristics and Origin. International Geology Review, 38, 1098-1133.

Malpas, J., 1979. Two contrasting trondhjemite associations from transported ophiolites in Western Newfoundland. In: Barker, F. (ed.). Trondhjemites, Dacites, and Related Rocks. Amsterdam, Elsevier, 465-487.

Martin, H., 1986. Effect of steeper geothermal gradient on geochemistry of subduction zone magmas. Geology, 14, 753-756.

Montgomery, H., Pessagno, E.A., Jr, Lewis, J.F., Schellekens, J.H., 1994. Paleogeography of Jurassic fragments in the Caribbean. Tectonics, 13, 725-732.

Morris, P.A., 1995. Slab melting as an explanation of Quaternary volcanism and aseismicity in southwest Japan. Geology, 23, 395-398.

Nash, W.P., Crecraft, H.R., 1985. Partition coefficients for trace elements in silicic magmas. Geochimica et Cosmochimica Acta, 49, 309-322.

Nicholls, G.T., Wylie, P.J., Stern, C.R., 1994. Subduction zone melting of pelagic sediments constrained by melting experiments. Nature, 371, 785-788.

Peacock, S., 1993. Large-scale hydration of the lithosphere above subducting slabs. Chemical Geology, 108, 49-59.

Pallister, J.S., Knight, R.J., 1981. Rare-earth element geochemistry of the Samail ophiolite near Ibra, Oman. Journal of Geophysical Research, 86, 2673-2697.

Pearce, J.A., 1983. Role of subcontinental lithosphere in magma genesis at active continental margins. In: Hawkesworth, C.J., Norry, M.J. (eds.). Continental Basalts and Mantle Xenoliths. Natwich, Shiva, 373-403.

Pearce, J.A., Harris, N.B.W, Tindle, A.G., 1984. Trace element discrimination diagrams for the tectonic interpretation of granitic rocks. Journal of Petrology, 25, 956-982.

Pearce, J.A., Parkinson, I.J., 1993. Trace element models for mantle melting: application to volcanic arc petrogenesis. Geological Society of London Special Paper, 76, 373-403.

Pearce, J.A., Baker, P.E., Harvey, P.K, Luff, I. W., 1995. Geochemical evidence for subduction fluxes, mantle melting and fractional crystallization beneath the South Sandwich Island Arc. Journal of Petrology, 36, 1073-1109.

Pearce, J.A., Kempton, P.D., Nowell, G.M., Nobel, S.R., 1999. Hf-Nd element and isotope perspective on the nature and provenance of mantle and subduction components in Western Pacific arc-basin systems. Journal of Petrology, 40, 1579-1611.

Pessagno, E.A., 1976. Middle Cretaceous planktonic foraminifera of the Antilles-Caribbean region and eastern Mexico. Musée d'Historie Naturelle de Nice, Annales, 4, 176-182.

Pindell, J.L., Barrett, S.F., 1990. Geological evolution of the Caribbean region: a plate tectonic perspective. In: Dengo, G., Case, J.E. (eds.). The Caribbean Region. Geological Society of America Special Paper, H, 405-432.

Plank, T., Langmuir, C.H., 1998. The chemical composition of subducting sediment and its consequences for the crust and mantle. Chemical Geology, 145, 325-394.

Price, R.C., Gamble, J.A., Smith, I.E.M., Stewart, R.B., Eggins, S., Wright, I.C., 2005. An integrated model for temporal evolution of andesites and rhyolites and crustasl development in New Zealand's North Island. Journal of Volcanology and Geothermal Research, 10, 1-24.

Proenza, J.A., Díaz-Martínez, R., Iriondo, A., Marchesi, C., Melgarejo, J.C., Gervilla, F., Garrido, C.J., Rodriguez-Vega, A., Lozano-Santacrus, R., Blanco-Moreno, J.A., 2006. Primitive Cretaceous island-arc volcanic rocks in eastern Cuba: the Téneme Formation. Geologica Acta, 4, 103-121.

Prouteau, G., Scallet, B., Pichavant, M., Maury, R.C., 2001. Evidence for mantle metasomatism by hydrous silicic melts derived from subducted oceanic crust. Nature, 410, 197-200.

Rankin, D., 2002. Geology of St. John, U.S. Virgin Islands. United States Geologicl Survey Professional Paper, 1631, 1-36.

Rapp, R. P., Watson, E.B., 1995. The amphibole-out phase boundary in partially melted metabaslat at 8-32 kbar: implications for continental growth and crust-mantle recycling. Journal of Petrology, 36, 891-931.

Rapp, R.P., Shimizu, N., Norman, M.D., Applegate, G.S., 1999. Reaction between slab-derived melts and peridotite in the mantle wedge: experimental constraints at 3.8 GPa. Chemical Geology, 160, 335-356.

Rollinson, H., 1993. Using Geochemical Data: Evaluation, Presentation, Interpretation. London, Longman, 352 pp.

Ryerson, F.J., Watson, E.B., 1987. Rutile saturtion in magmas: implications for Ti-Nb-Ta depletion in island-arc basalts. Earth and Planetary Science Letters, 86, 225-239.

Sajona, F.G., Bellon, H., Maury, R.C., Pubellier, M., Cotten, J., Rangin, C., 1994. Magmatic response to abrupt changes in geodynamic settings: Pliocene-Quaternary calc-alkaline and Nb-enriched lavas, Mindanao (Philippines). Tectonophysics, 237, 47-72.

Schellekens, J.H., Montgomery, H., Joyce, J., Smith, A.L., 1990. Late Jurassic to Late Cretaceous development of island arc crust in southwestern Puerto Rico. Transactions of 12th Caribbean Geological Conference, St. Croix, U.S. Virgin Islands, The University of Miami, FL, 268-281,

Schellekens, J.H., 1998. Geochemical evolution and tectonic history of Puerto Rico. In: Lidiak, E.G., Larue, D. K. (eds.). Tectonics and Geochemistry of the Northeastern Caribbean. Geological Society of America Special Paper, 322, 35-66

Schiano, P., Clocchiatti, R., 1994. Worldwide occurrence of silica-rich melts in suib-continental and sub-oceanic mantle minerals. Nature, 368, 621-624.

Schiano. P., Cloccjiatti, R., Shimizu, N., Maury, R.C., Jochum, K.P., Hoffman, A.W., 1995. Hydrous silica-rich melts in the sub-arc mantle and their relationship with erupted arc lavas. Nature, 377, 594-600.

Sen, C., Dunn, T., 1994. Experimental modal metasomatism of a spinel lherzolite and the production of amphibole-bearing peridotite. Contributions to Mineralogy and Petrology, 119, 422-432.

Shaw, D.M., 1970. Trace element fractionation during anatexis. Geochimica et Cosmochimica Acta, 34, 237-43.

Sisson, T.W., 1991. Pyroxene-high silica rhyolite trace element partition coefficients measured by ion microprobe. Geochimica et Cosmochimica Acta, 55, 1575-1585.

Smith, I.E.M., Stewart, R.B., Price, R.C., 2003. The petrology of a large intra-oceanic silicic eruption: the Sandy Bay Tephra, Kermadec Arc, Southwest Pacific. Journal of Volcanology and Geothermal Research, 124, 173-194.

Smithies, R.H., 2000. The Archaean tonalite-trondhjemite-granodiorite (TTG) series is not an analogue of Cenozoic adakite. Earth and Planetary Science Letters, 182, 115-125.

Spiegelman, M., McKenzie, D., 1987. Simple 2-d models for melt extraction at mid-ocean ridges and island arcs. Earth and Planetary Science Letters 156, 139-167.

Stern, C.R., Kilian, R., 1996. Role of subducted slab, mantle wedge and continental crust in the generation of adakites from the Andean Austral Volcanic Zone. Contributions to Mineralogy and Petrology, 123, 263-381.

Stimac, J., Hickmott, D., 1994. Trace-element partition-coefficients for ilmenite, orthopyroxene and pyrrhotite in rhyolite, detrermined by micro-pixe analysis. Chemical Geology, 117, 313-330.

Sun, S.-S., McDonough, W.F., 1989. Chemical and Isotopic systematics of oceanic basalts. In: Saunders, A., Norry, M. (eds.). Magmatism in Ocean Basins, Geological Society Special Publication, 42, 313-45.

Tamura, Y., Tatsumi, Y., 2002. Remelting of andesitic crust as possible origin of rhyolite in oceanic arcs: an example from Izu-Bonin Arc. Journal of Petrology, 43, 1029-1047.

Tatsumi, Y., Shukuno, H., Sato, K., Shibata, T., Yoshikawa, M., 2003. The petrology and geochemistry of high-magnesium andesites at the western tip of the Setouchi Volcanic Belt, SW Japan. Journal of Petrology, 44, 1562-1578.

Thy, P., Lofgren, G.E., 1994. Experimental constraints on the low-pressure evolution of transitional and mildly alkalic basalts: the effect of Fe-Ti oxide minerals, and the origin of basaltic andesites. Contributions to Mineralogy and Petrology, 116, 340-351.

Toplis, M.J., Carroll, M.R., 1995. An experimental study of the influence of oxygen fugacity on Fe-Ti oxide stability, phase relations, and mineral-melt equilibria in ferro-basalt systems. Journal of Petrology, 36, 1137-1170.

Tsvetlov, A.A., 1991. Magmatism of the westernmost (Komandorsky) seqment of the Aleutian island arc. Tectonophysics, 199, 289-317.

Wyllie, P.J., Wolf, M.B., 1993. Amphibolite dehydration-melting: Sorting out the problem. In: Alabaster, H.M., Harris, N.B.W., Neary, C.R. (eds.). Magmatic Processes and Plate Tectonics. Geological Society Special Publication, 76, 405-416.

Woodhead, J., Eggins, S., Johnson, R., 1998. Magma genesis in New Britain: Further insights into melting and mass transfer processes. Journal of Petrology, 39, 1641-1668.

Yazeva, R.G., 1978. Sodic acidic volcanites of the Urals and plagiorhyolites of recent island arcs. International Geology Review, 20, 1009-1020.

Yogodzinski, G.M., Volynets, A.V., Koloskov, A.V., Seliverston, N.I., Matvenkov, V.V., 1994. Magnesian andesites and the subduction component in a strongly calc-alkaline series at Piip Volcano, Far Western Aleutians. Journal of Petrology, 35, 163-204.

Yogodzinski, C.A., Kay, R.W., Volynets, O., Koloskov, A., Kay, S.M., 1995. Magnesian andesite in the western Aleutians: Implications for slab melting processes in the mantle wedge. Geological Society of America Bulletin, 107, 505-519.

Manuscript received January 2005;
revision accepted October 2005.

APPENDIX

Major and trace element analyses of basalts and plagiorhyolites from the Water Island Formation, Virgin Islands. Data listed are absolute values determined by ICP techniques.

TABLE 1 | **Major and trace element analyses of Water Island basalts and plagiorhyolites.**

Sample	WIST	WIST	WISJ	WISJ	WIST	WIST	WISJ	WISJ	WIST	WIST
Number	44	76HB	144	24	68	68B	87	39	33	RH251
Unit	1	1	1	1	1	1	1	1	1	1
SiO_2	43.78	47.04	47.65	48.13	48.62	48.72	49.96	50.85	51.23	53.12
TiO_2	0.55	0.51	0.6	0.55	0.44	0.44	0.6	0.73	0.61	0.56
Al_2O_3	14.12	17	15.42	14.58	16.09	16.14	17.03	18.28	15.51	15
Fe_2O_3	7.59	10.37	9.13	9.31	8.8	8.72	9.67	11.1	9.49	6.76
MnO	0.3	0.11	0.14	0.11	0.09	0.09	0.12	0.17	0.12	0.13
MgO	4	7.74	9.43	9.83	7.49	7.54	6.16	4.95	6.33	6.76
CaO	13.77	6	8.45	11.2	7.26	7.29	11.55	7.78	11.29	7.22
Na_2O	4.43	1.7	2.29	2.06	3.53	3.44	1.65	4.14	1.8	2.7
K_2O	0.08	1.64	0.31	0.14	0.05	0.04	0.21	0.3	0.34	0
P_2O_5	0.07	0	0.05	0.04	0.03	0.04	0.05	0.03	0.05	0.04
Subtot.	87.93	91.07	92.56	95.02	91.52	91.59	96.03	97.22	95.82	91.61
LOI	11	7.2	6.3	3.8	7.6	7.3	2.7	1.5	3.1	6.2
Cr	0	48	151	7	0	0	82	0	14	48
Ni	20	43	63	78	23.2	23.5	17.7	20	44	52
Co	32.7	31.2	36	43.1	31.7	33.9	34.7	31.7	36.4	34.2
Sc	32	46	41	47	36	37	48	44	38	36
V	341	229	230	295	260	267	329	465	309	275
Cu	66	0	0	138	89	84.6	115.6	101.6	15.8	60
Pb	1.6	2.46	2.1	0.6	0.8	0.8	0.7	0.4	0.4	1.72
Zn	103	0	0	48	60	59	58	48	38	65
Rb	2.5	35.8	4.4	2.2	1	1.2	2.8	8.4	5.3	8.1
Cs	0.5	0.6	0.4	0.1	0.2	0	0.2	0.9	0.7	0.3
Ba	90	133	62	17	20	9	70	68	50	83
Sr	146.7	13.9	137.3	218.4	181.4	180.5	226.7	136.2	100.3	164.8
Ga	15.6	13.9	13.5	16.5	13.3	14.7	17.5	16.3	14.9	13.4
Ta	0.03	0.033	0	0.02	0.02	0	0	0.03	0.02	0
Nb	0.5	0.5	0	0.3	0.4	0	0	0.5	0.3	0
Hf	0.7	0.7	0.7	1	0.7	0.7	0.9	0.9	0.8	0.5
Zr	19.1	16.5	23.2	23.1	18.3	19	15.3	25.6	24.5	18.9
Y	8.5	7.7	13.5	12	8.7	8.2	10.6	13.8	13.2	11.9
Th	0.5	0	0.2	0.1	0.2	0.2	0	0.2	0.1	0.2
U	0.8	0	0.1	0.6	0.1	0	0.7	0.7	0.1	0.1
La	2.2	0	1.3	1.1	0.9	0.8	1.2	1.9	1.2	0.8
Ce	4.2	0	3.2	3.5	2.2	2.2	2.9	3.7	2.8	1.9
Pr	0.74	0.3	0.77	0.6	0.36	0.41	0.56	0.73	0.67	0.6
Nd	4.3	1.9	4.3	3.6	2.1	2	3.1	4	4	3.4
Sm	1.3	0.6	1.4	1.1	0.8	0.9	1	1.4	1.2	1.2
Eu	0.45	0.28	0.51	0.53	0.31	0.34	0.6	0.53	0.56	0.5
Gd	1.35	1.05	1.9	1.77	1.31	1.27	1.56	2.04	1.97	1.52
Tb	0.23	0.2	0.34	0.27	0.2	0.24	0.28	0.32	0.34	0.32
Dy	1.42	1.21	2.27	2.02	1.48	1.56	1.84	2.08	2.12	1.68
Ho	0.31	0.29	0.49	0.43	0.32	0.33	0.4	0.49	0.49	0.47
Er	0.95	0.92	1.37	1.41	0.92	0.89	1.24	1.51	1.37	1.2
Tm	0.13	0.13	0.21	0.19	0.14	0.14	0.18	0.2	0.21	0.18
Yb	0.93	1.01	1.18	1.32	0.83	1.03	0.96	1.52	1.27	1.18
Lu	0.15	0.15	0.19	0.22	0.12	0.14	0.18	0.22	0.25	0.2

TABLE 1 | **Continued.**

Sample	**WISJ**	**WISJ**	**WISJ**	**WIST**	**WIST**	**WISJ**	**WIST**	**WIST**	**WIST**	**WIST**
Number	**88**	**89**	**68-15**	**31**	**32**	**38**	**35**	**29**	**66**	**36**
Unit	**2**	**2**	**3**	**3**	**3**	**4**	**4**	**4**	**4**	**4**
SiO_2	45.40	47.63	43.94	48.04	51.91	64.24	67.57	77.95	76.66	82.06
TiO_2	0.57	0.56	0.56	0.49	0.45	0.46	0.56	0.25	0.28	0.12
Al_2O_3	16.11	15.95	14.24	17.06	16.12	15.62	14.83	11.99	8.89	9.75
Fe_2O_3	8.85	9.44	8.84	9.73	8.99	5.54	5.01	1.78	5.05	1.62
MnO	0.15	0.14	0.17	0.12	0.08	0.06	0.05	0.01	0.07	0.02
MgO	5.48	6.16	6.99	8.78	6.63	3.12	1.81	0.04	2.09	0.31
CaO	14.5	10.1	11.04	6.09	8.16	5.56	2.65	0.18	1.22	0.69
Na_2O	1.64	3.28	4.27	1.94	3.28	2.5	4.43	6.28	2.98	3.75
K_2O	0.06	0.46	0.46	0.46	0.07	0.08	0.45	0.66	0.19	0.77
P_2O_5	0.03	0.05	0.06	0.01	0.03	0.18	0.1	0.04	0.06	0.01
Subtot.	91.9	92.82	89.69	91.75	94.82	96.8	96.96	99	96.98	98.94
LOI	7.2	5.9	9.2	4.2	4.2	2.5	2.4	0.8	2.3	0.8
Cr	0	95	144	35	0	0	0	0	0	0
Ni	15.8	15.9	45	29	30	30	20	32	1.6	20
Co	31.7	34.9	30.2	37.3	36.5	10.8	7	1.3	8.6	1.1
Sc	43	48	38	54	40	19	23	8	18	4
V	301	295	241	286	271	86	24	9	26	7
Cu	85.6	98.3	0	157.5	7.4	30.5	1.7	6	9.6	4.
Pb	4.8	0.8	2.06	0.7	0.2	0.3	1.6	3	1.1	0.4
Zn	57	67	0	67	49	45	118	10	112	8
Rb	0.9	9.2	6.7	9.9	1	2.5	8	5.7	2.7	14.3
Cs	0.1	0.2	0.7	1	0.1	0.5	0.5	0.3	0	0.5
Ba	46	124	129	117	14	85	85	45	50	391
Sr	205.2	297.6	252	212.4	164.1	274.4	80.8	30.5	55.7	159.3
Ga	15.7	14.6	11.3	16.8	14.5	15.2	17	14.3	11	8.9
Ta	0	0	0	0.03	0.03	0.03	0.02	0.04	0	0.03
Nb	0	0	0.6	0.6	0.5	0.5	0.4	0.7	0.5	0.5
Hf	0.6	0.7	0.7	0.7	0.7	1.8	1.7	2.7	2	2.8
Zr	14	12.7	19.9	17.1	19.4	38	45.2	68.6	58.6	73
Y	12.9	12.8	11.4	7.7	11.2	17.3	26.5	30.8	34.7	22.2
Th	0.2	0	0	0.1	0.3	0.3	0.4	0.3	0.1	1
U	0.1	0.5	0.4	0.2	0.2	0.8	0.9	1	0.2	0.6
La	1	0.9	0.7	0.9	1	3.9	2.4	3.8	6.7	4.5
Ce	2.6	2.4	1.6	3.2	3.4	9	5.3	10	13.6	10.6
Pr	0.54	0.47	0.61	0.56	0.44	1.74	1.1	1.68	2.3	1.7
Nd	2.8	2.3	4.1	2.7	2.8	9.4	6.6	9	13.8	8.1
Sm	1.1	1.1	1.2	1	1.1	2.4	2.5	2.7	3.4	2.4
Eu	0.44	0.53	0.47	0.39	0.46	0.97	0.95	0.99	1.48	0.21
Gd	1.76	1.37	1.57	1.13	1.63	2.94	3.68	3.96	4.67	2.73
Tb	0.33	0.3	0.29	0.18	0.26	0.43	0.62	0.66	0.82	0.45
Dy	2.07	1.84	1.58	1.5	1.69	2.82	3.81	5.08	4.78	3.13
Ho	0.46	0.5	0.38	0.29	0.35	0.59	0.89	1.06	1.06	0.71
Er	1.4	1.35	1.1	0.94	1.11	1.76	2.82	3.3	2.87	2.16
Tm	0.19	0.19	0.19	0.17	0.16	0.26	0.43	0.5	0.41	0.4
Yb	1.42	1.67	1.06	1	1.07	1.74	2.58	3.3	3.06	2.4
Lu	0.19	0.2	0.18	0.17	0.16	0.26	0.37	0.53	0.53	0.42

TABLE 1 **Continued.**

Sample	**WISJ**	**WIST**	**WISJ**	**WISJ**	**WISJ**	**WISJ**	**WISJ**	**WISJ**	**WIST**	**WIST**	**WISJ**	**WIST**
Number	**23**	**27**	**94**	**22**	**20**	**25**	**21**	**14**	**43**	**37**	**16**	**7**
Unit	**5**	**5**	**5**	**5**	**5**	**5**	**5**	**5**	**5**	**5**	**5**	**5**
SiO_2	64.75	64.83	67.02	70.22	71.64	73.27	73.5	74.34	74.28	76.96	76.07	75.32
TiO_2	0.37	0.87	0.47	0.5	0.33	0.33	0.37	0.31	0.28	0.14	0.26	0.29
Al_2O_3	14.66	13.79	15.33	12.79	12.71	13.15	12.04	12.76	12	13.11	12.18	12.34
Fe_2O_3	5.43	5.98	5.02	3.98	2.88	3.16	3.19	2.54	2.44	1.98	2.21	2.1
MnO	0.06	0.04	0.06	0.05	0.07	0.08	0.03	0.04	0.08	0.02	0.01	0.01
MgO	5.61	2.91	1.62	4.44	1.01	0.78	2.21	1.01	0.82	0.22	0.86	1.1
CaO	4.85	1.43	2.95	0.5	2.06	1.84	0.8	1.45	1.66	0.79	0.98	0.46
Na_2O	2.46	6.58	4.79	1.93	5.61	3.9	5.66	5.56	4.08	4.95	5.73	3.03
K_2O	0.08	0.05	2.27	1.88	0.83	2.56	0.2	0.48	1.77	1.44	0.22	2.29
P_2O_5	0.03	0.16	0.09	0.05	0.03	0.03	0.05	0.03	0.02	0.01	0.04	0.02
Subtot.	97.76	96.04	99.12	95.94	96.88	98.78	97.73	98.27	97.19	98.15	98.34	96.05
LOI	2.4	3	0.4	3.8	2.6	0.7	1.8	1.2	2.3	1.5	1.2	1.5
Cr	14	0	0	0	0	0	0	0	0	7	0	0
Ni	109	20	3.4	50	35	31	55	40	20	20	43	20
Co	20.7	9.6	11.6	2.5	3.1	4	2.8	5.3	2	1.2	4.3	1.2
Sc	25	21	20	15	11	11	14	12	8	5	7	9
V	145	91	103	14	16	38	22	29	14	9	13	8
Cu	75	3	14.5	3	3	5	4	9	3.7	4.2	3	3.4
Pb	1.3	2	1	1.5	1.6	1.4	2.7	1.3	0.5	3.3	2	1
Zn	37	101	52	76	60	32	48	169	31	11	5	30
Rb	0.8	0.6	29	17	9.1	18.6	2.1	5.2	15.6	20.4	1.9	19.3
Cs	0.1	0.1	0.3	0.4	0.1	0.1	0.1	0.1	0.2	0.6	0.1	0.2
Ba	13	21	385	225	102	273	24	103	357	330	95	319
Sr	44.8	45.1	174.6	27.9	102.4	163.5	102.1	73.4	100.3	33.2	131.6	72.5
Ga	17.5	20.4	15.5	18.1	16.3	15.1	14.6	12.6	11	14.6	11.9	14.4
Ta	0.04	0.05	0	0.04	0.05	0.06	0.05	0.05	0.03	0.05	0.06	0.04
Nb	0.7	0.9	0.8	0.7	0.9	1.1	0.9	0.8	0.6	0.8	1.1	0.7
Hf	2.6	3.2	1.8	2.6	3.1	3.5	4.2	3	2.9	3.4	4.1	2.9
Zr	73.4	82.2	62.4	70.4	86.6	90.5	104	82.7	87.9	89.5	95.5	94
Y	22.8	31	22	23	23.7	22.4	30.7	21.2	20.4	28.1	28.3	26
Th	0.4	0.2	0.2	0.5	0.7	1.1	0.5	0.8	1.2	1.8	0.7	1.2
U	0.1	0.5	0.4	0.3	0.3	0.5	0.4	0.4	0.6	0.5	0.4	0.5
La	3.6	4.3	3.6	2.8	2.8	6.5	5.1	4.5	5.3	7.4	5.3	6.8
Ce	10.8	12.2	8.7	8	8	14.6	15.2	10.1	13	16.2	14	15.5
Pr	1.65	1.97	1.52	1.36	1.21	1.98	2.53	1.51	2.01	2.51	2.11	2.6
Nd	8.8	11.2	8.8	7.4	6	9	13.5	7.3	10.3	11.8	10.1	12.4
Sm	2.2	3.5	2.3	2.1	2.1	2.6	3.7	2.2	2.6	2.8	3.1	3.4
Eu	0.84	1.28	0.87	0.78	0.4	0.75	1.4	0.64	0.72	0.33	0.8	0.88
Gd	2.95	4.44	3.27	2.88	2.56	2.85	5.05	2.51	3.22	3.23	3.63	3.75
Tb	0.51	0.79	0.59	0.5	0.47	0.49	0.87	0.43	0.49	0.58	0.63	0.55
Dy	3.47	5.44	3.7	3.73	3.42	3.49	6.04	3.33	3.01	3.89	4.23	3.64
Ho	0.73	1.06	0.85	0.76	0.74	0.73	1.35	0.67	0.69	0.85	0.94	0.83
Er	2.38	3.37	2.41	2.54	2.59	2.29	4.27	2.16	2.02	2.93	3.12	2.59
Tm	0.35	0.51	0.37	0.38	0.43	0.37	0.64	0.36	0.31	0.48	0.49	0.41
Yb	2.38	3.41	2.52	2.74	2.77	2.6	4.54	2.42	2.27	3.27	3.37	2.66
Lu	0.39	0.5	0.38	0.43	0.43	0.47	0.69	0.38	0.39	0.52	0.53	0.42

TABLE 2 **Major and trace element analyses of MORB tholeiite and amphibolite, Sierra Bermeja Complex, Western Puerto Rico.**

Sample Number	AMPH 30	CAJ D	CAJ E	CAJ A	CAJ B	CAJ C	CAJDS 103B	LCAJ Z	LCAJ Y	LCAJ X	LCAJ V	LCAJ U
SiO_2	64.75	64.83	67.02	70.22	71.64	73.27	73.5	74.34	74.28	76.96	76.07	75.32
SiO_2	48.79	49.65	68.98	66.16	68.50	54.19	51.45	46.29	53.00	53.48	45.21	69.45
TiO_2	0.71	1.89	1.50	1.44	1.57	1.79	1.05	1.22	1.46	1.71	1.26	1.60
Al_2O_3	12.09	13.55	9.63	10.62	10.00	11.92	15.09	12.88	13.52	10.85	12.82	9.46
Fe_2O_3	9.64	12.38	6.71	9.18	8.22	13.57	9.96	9.11	11.02	12.78	9.26	7.35
MnO	0.15	0.21	0.07	0.10	0.08	0.15	0.19	0.18	0.17	0.15	0.18	0.08
MgO	17.04	6.99	1.80	2.13	1.58	4.81	7.70	10.24	6.63	4.91	11.82	1.61
CaO	9.40	8.78	4.98	4.88	4.81	6.44	10.03	15.48	8.22	9.75	14.21	5.26
Na_2O	1.46	2.99	3.56	3.48	3.77	4.06	3.09	0.45	3.64	2.26	0.37	3.06
K_2O	0.05	0.71	0.24	0.18	0.28	0.56	0.77	0.10	0.47	0.07	0.09	0.13
P_2O_5	0.05	0.15	0.35	0.32	0.38	0.17	0.08	0.12	0.15	0.17	0.13	0.36
Subtot.	98.41	96.06	97.15	97.57	98.37	96.30	98.41	95.16	97.18	94.85	94.42	97.62
LOI	0.05	2.60	2.10	1.40	0.70	2.20	0.03	3.90	1.60	3.80	4.60	1.60
Ni	700.7	34.6	10.9	11.2	16.3	24.8	50.3	28.5	33.3	22.9	42.7	11.3
Co	0.0	47.7	17.2	19.4	18.1	32.4	0.0	33.1	36.4	30.9	34.2	17.3
Sc	39	43	24	20	21	38	39	32	37	39	33	23
V	216	429	182	169	189	368	281	263	340	342	258	176
Cu	61.0	69.9	39.9	38.2	57.6	34.8	52.7	144.5	91.5	39.9	52.5	40.0
Pb	2.0	1.9	1.9	1.0	0.6	1.8	0.7	9.1	18.4	3.4	16.7	5.6
Zn	42	83	113	80	102	83	55	16	24	80	21	89
Rb	0.2	12.7	4.6	2.0	5.1	9.8	12.4	1.0	9.0	0.0	0.8	1.9
Cs	0.0	0.1	0.1	0.0	0.1	0.0	0.0	0.0	0.3	0.0	0.0	0.0
Ba	115.8	399.0	64.0	324.0	42.0	71.0	217.4	48.0	576.2	185.2	26.0	25.1
Sr	296.2	169.5	56.4	102.7	73.6	96.0	256.7	24.7	164.8	30.1	26.8	42.1
Ga	11.9	18.8	15.8	20.0	19.2	16.8	14.6	13.9	17.7	17.9	14.1	16.8
Ta	0.0	0.3	0.8	0.6	0.7	0.3	0.0	0.0	0.1	0.1	0.1	0.5
Nb	0.9	3.6	8.8	9.3	9.2	3.0	1.5	1.8	1.3	2.1	1.4	7.6
Hf	1.1	3.3	8.3	10.3	9.7	4.8	1.9	1.9	2.5	2.6	2.1	8.2
Zr	37.0	101.0	290.0	355.5	355.0	129.1	64.7	67.9	80.9	86.9	74.1	269.1
Y	14.6	46.2	97.9	110.1	111.7	48.1	22.1	27.5	36.0	46.8	29.3	91.1
Th	0.05	0.50	1.00	1.10	2.00	0.20	0.18	0.00	0.00	0.00	0.30	1.10
U	0.0	1.0	0.8	0.1	0.4	0.0	0.0	0.0	0.0	0.0	0.0	0.4
La	1.46	4.30	13.60	16.10	15.30	5.40	2.62	3.30	3.20	3.40	3.40	11.90
Ce	4.3	12.4	41.2	44.0	44.4	16.0	7.8	9.2	10.4	11.4	10.5	35.3
Pr	0.75	2.11	6.44	7.18	7.34	2.51	1.31	1.60	1.78	1.95	1.73	5.81
Nd	3.96	12.20	36.70	38.00	36.00	14.70	7.19	8.80	10.80	11.50	9.90	32.80
Sm	1.4	4.3	10.3	11.7	12.7	4.7	2.7	2.6	3.1	3.7	2.9	9.8
Eu	0.58	1.66	2.58	2.63	2.91	1.38	0.91	1.10	1.30	1.33	1.41	2.36
Gd	2.09	5.99	14.02	14.35	15.85	6.13	3.24	3.90	4.63	5.63	4.13	12.91
Tb	0.33	1.13	2.59	2.67	2.92	1.27	0.54	0.70	0.87	0.93	0.78	2.31
Dy	2.56	7.29	15.78	17.55	18.82	8.24	4.12	4.38	5.80	6.70	4.64	14.84
Ho	0.53	1.76	3.44	3.74	3.77	1.83	0.85	0.92	1.24	1.49	0.92	3.10
Er	1.57	4.68	9.55	11.58	12.01	5.46	2.38	2.77	3.51	4.53	3.01	9.02
Tm	0.24	0.68	1.52	1.58	1.62	0.76	0.36	0.40	0.52	0.74	0.44	1.38
Yb	1.55	4.52	9.42	10.00	10.27	4.66	2.33	2.66	3.41	4.50	2.75	9.22
Lu	0.24	0.68	1.35	1.56	1.46	0.73	0.37	0.43	0.58	0.70	0.45	1.37

TABLE 3 | **Mass balance calculations reveal removal of appropriate proportions of observed phenocryst phases (est. ol, olivine; analysed cpx, augite; analysed pl, plagioclase; est. mt, titanomagnetite) from parent basalt 87 (Table 1) produces daughter plagiorhyolite 23 with low sum of squares of residuals (SR2). Data in wt.%.**

Element Sample	Parent 87	Calc.	Diff.	ol fo78	cpx 18B	pl 18B	mt (Fe-Ti)	Daughter 23
SiO2	52.02	52.09	0.07	38.14	50.90	45.22	0.23	66.24
TiO2	0.62	0.82	0.19	0.01	0.66	0	8.40	0.38
Al2O3	17.73	17.80	0.07	0.02	4.58	34.03	4.82	15.00
FeO*	9.06	9.10	0.04	20.82	6.84	0.78	81.71	5.00
MgO	6.41	6.47	0.06	40.74	15.10	0	2.52	5.74
MnO	0.12	0.05	0.07	0.35	0	0	0.36	0.06
CaO	12.03	12.06	0.03	0.18	19.90	17.78	0	4.96
Na2O	1.72	1.49	0.23	0.01	0.20	1.51	0	2.52
K2O	0.22	0.04	0.18	0	0	0.02	0	0.08
Coeff				0.02	0.23	0.31	0.06	0.39
SR^2	0.143							

TABLE 4a | **Summary of petrogenetic constraints, Water Island Formation basaltic subunits.**

Basaltic subunits	Source	Evidence	% melting	Evidence	% sediment	Evidence	% Crustalt component	Evidence
WIVI-1 & 2	RMM2-5	Nb-Yb Ti-Fe*/Mg Cr-Yb	25	Nb-Yb Cr-Yb	<0.5-1.5	La/Nb-Nb/Zr $(Ce/Ce^*)_N$	Mostly low	$(Ce/Ce^*)_N$
WIVI-3	FMM	Nb-Yb La/Nb	5-15	Nb-Yb La/Nb	0-0.5	La/Nb-Nb/Zr $(Ce/Ce^*)_N$	0	La/Nb-Nb/Zr

TABLE 4b | **Summary of petrogenetic constraints, Water Island Formation plagiorhyolite subunits.**

Plagiorhyolite subunit	Source	Evidence	% Melt	Evidence	% sediment	Evidence
4a. Low-HFSE Flat LREE	Alt. gabbro and amph.	Mg#-SiO_2 Sr-Y, Sr-Mg# REE model	15-25	REE model Zr/Sm-Sm/YbN	Small	La/Nb-Nb/Zr (Ce/Ce*)
4b. Low-HFSE Ce anomaly	Alt. gabbro	"	15-25	REE model Zr/Sm-Sm/Yb	Small	La/Nb-Nb/Zr $(Ce/Ce^*)_N$
5a. High-HFSE Enr LREE	Amph.	Mg#-SiO_2 Sr-Y, Sr-Mg# REE model	25-50	REE model La/Sm-Sm/Yb	Negligible	La/Nb-Nb/Zr $(Ce/Ce^*)_N$
5b. High-HFSE Depl LREE	Alt. gabbro	"	15-25	REE model La/Sm-Sm/Yb	Negligible	La/Nb-Nb-Z $(Ce/Ce^*)_N$